Northumbria Research Link

Journal Pre-proof

Quaternary environmental evolution in the South Carpathians reconstructed from glaciokarst geomorphology and sedimentary archives

Laura Tîrlă, Virgil Drăgușin, Petra Bajo, Silviu Covaliov, Nicolae Cruceru, Vasile Ersek, Diana Hanganu, John Hellstrom, Dirk Hoffmann, Ionuț Mirea, Tiberiu Sava, Gabriela Sava, Ionuț Șandric

Please cite this article as: L. Tîrlă, V. Drăgușin, P. Bajo, et al., Quaternary environmental evolution in the South Carpathians reconstructed from glaciokarst geomorphology and sedimentary archives, *Geomorphology*(2020), https://doi.org/10.1016/j.geomorph.2020.107038

This is a PDF file of an article that has undergone enhancements after acceptance, such as the addition of a cover page and metadata, and formatting for readability, but it is not yet the definitive version of record. This version will undergo additional copyediting, typesetting and review before it is published in its final form, but we are providing this version to give early visibility of the article. Please note that, during the production process, errors may be discovered which could affect the content, and all legal disclaimers that apply to the journal pertain.
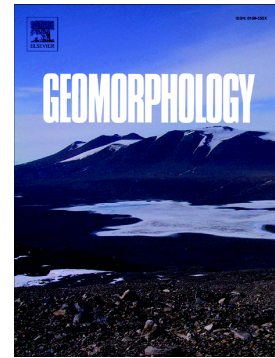
Quaternary environmental evolution in the South Carpathians reconstructed from glaciokarst geomorphology and sedimentary archives

Laura Tîrlă[1,2], Virgil Drăgușin[3], Petra Bajo[4,5], Silviu Covaliov[6], Nicolae Cruceru[3], Vasile Ersek[7], Diana Hanganu[8], John Hellstrom[5], Dirk Hoffmann[9], Ionuț Mirea[3,10], Tiberiu Sava[11], Gabriela Sava[11], Ionuț Şandric[1,2,12]

[1] University of Bucharest, Faculty of Geography, N. Bălcescu 1, Bucharest, Romania

[2] Research Institute of the University of Bucharest (ICUB), M. Kogălniceanu 36-46, Bucharest, Romania

[3] Emil Racoviță Institute of Speleology, Romanian Academy, Frumoasă St. 31, Bucharest, Romania

[4] Croatian Geological Survey, Milana Sachsa 2, Zagreb, Croatia

[5] School of Earth Sciences, The University of Melbourne, Parkville, Victoria 2010, Australia

[6] Danube Delta National Institute for Research and Development, Babadag St. 165, Tulcea, Romania

[7] Northumbria University, Department of Geography, Ellison Building, NE1 8ST, Newcastle upon Tyne, UK

[8] ArchaeoScience#RO Platform, Research Institute of the University of Bucharest (ICUB), M. Kogălniceanu 36-46, Bucharest, Romania

[9] Georg-August-Universität, Faculty of Geoscience and Geography, Department of Isotope Geology, Goldschmidtstraße 3, D-37077 Göttingen, Germany

[10] Babeş-Bolyai University, Department of Geology, M. Kogălniceanu 1, Cluj-Napoca, Romania

[11] Horia Hulubei National Institute for R&D in Physics and Nuclear Engineering, IFIN-HH, 30 Reactorului St., Măgurele, Romania

[12] ESRI Romania, Washington St. 25, Bucharest, Romania

Corresponding author: Laura Tîrlă, tirla@geo.unibuc.ro

Declaration of interests: The authors declare no conflict of interests.

1

1. INTRODUCTION

Glacial activity leaves geomorphological imprints on carbonate rock bodies isolated at high altitudes, resulting in what is known as the island type glaciokarst (Veress et al., 2019). Glaciated karst is a complex landscape, sensitive to climate change and capable of preserving unique evidence of past environmental change in alpine regions (Žebre and Stepišnik, 2015). The presence of speleothems, the most used paleoenvironmental archive found in karst, often indicate the existence of periods with optimal environmental conditions for their deposition, which at mid- and high-latitudes are restricted mostly to warm periods (McDermott, 2004). The initiation of cave formation itself, as resulting from a complex feedback between geology, geomorphology, climate, hydrology, and organic activity, is difficult to date but can be constrained using speleothem or clastic sediment deposition events (Polyak et al., 1998; Sasowsky, 1998; Stock et al., 2006; Häuselmann et al., 2015). The most common dating technique uses uranium series in speleothems (Richards and Dorale, 2003; Dorale et al., 2004; White, 2007; Scholz and Hoffmann, 2008), but trapped charge techniques such as OSL have also been used (Constantin et al., 2014).

In a glaciated environment, caves can be either truncated or completely removed by glaciation (Mais, 1999; Klimchouk et al., 2006), or be buried and preserved by infilling with glacial till (Cooper and Mylroie, 2015). They can also preserve morphological traits and sediments that could offer information useful for the reconstruction of mountain uplift (Meyer et al., 2011). Alpine caves and their associated sedimentary deposits brought more light onto the Quaternary evolution of the Alps (Spötl et al., 2002, 2007; Häuselmann et al., 2015), Apennines (Columbu et al., 2015), Norwegian Alps (e.g., Lauritzen, 1995; Berstad et al., 2002), or the Cantabrian Mountains (Ballesteros et al., 2015, 2019).

In Romania, glaciokarst does not reach a significant extent (Telbisz et al., 2019), but a handful of glaciokarst islands developed on carbonate rocks in the Rodnei and Parâng massifs (Teodorescu and Mitrofan, 1999), as well as Făgăraş (Mihai and Moldoveanu, 2006; Nedelea, 2006), and Piule-Iorgovanu (Ardelean, 2010) Mountains. However, especially owing to its scarcity, the Carpathian glaciokarst is significant due to the fact that it may preserve unique information about its tectonic and climatic history.

Late exhumation episodes during the Pleistocene favored a significant extent of glaciations in the Carpathians (Urdea, 2004). Glacial geomorphology of the Făgăraş Mountains supports the notion of at least two Pleistocene glacial phases (Florea, 1998; Mîndrescu and Evans, 2014).

Results of tectonic and thermochronological studies have shown that the paleoaltitudes were high since the latest Sarmatian (e.g., Răbăgia and Maţenco, 1999; Merten, 2011), but equilibrium line altitude (ELA) lowering earlier than the Middle Pleistocene was unlikely. The first evidence of two distinct glacial phases in the Bucegi Mountains were inferred by Micalevich (1959) from cave deposits in the Ialomiţa Cave.

Moreover, the inner-outer cirque pairs identified in several Carpathian massifs represent evidence of glaciations older than 130 ka (Mîndrescu, 2016). Nonetheless, the best-preserved glacial deposits date only since the Last Glacial Period (Reuther et al., 2007; Urdea et al., 2011; Kuhlemann et al., 2013; Ruszkiczay-Rüdiger et al., 2016). The last deglaciation has significantly contributed to the development of present-day alpine landscape in the central Făgăraş Mountains (Kuhlemann et al., 2013; Popescu et al., 2017). [10]Be analysis of the glacial moraines from Capra Valley indicated exposure ages of 17 ± 3.1 ka in the frontal part to 12.6 ± 2.0 ka in the glacial cirque (Kuhlemann et al., 2013).

This study focuses on the geological conditioning of karst and glacial relief development on the marble stripes of the central Făgăraş Mountains in the high-altitude South Carpathians (>2000 m), defined by present-day average uplift rates of about 2-3 mm yr^{-1} (Zugrăvescu et

al., 1998). We investigated tectonic features at different scales, as well as geomorphological traits based on a high-resolution digital elevation model (DEM).

We present uranium-thorium ages and carbon stable isotope data from several speleothems retrieved from caves from around 2400 m altitude, and radiocarbon dates of a doline's sedimentary infill.

In addition to bringing new data on the morphology and genesis of the Carpathian glaciokarst, our study also evaluates the reliability of karst sedimentary archives for future paleoenvironmental studies.

2. GEOLOGICAL AND GEOMORPHOLOGICAL FRAMEWORK

The central Făgăraș Mountains host an isolated marble karst with superimposed glacial features in the Mușeteica-Buda area, where dolomitic-calcitic marbles outcrop on an area of about 3 km^2 (Fig. 1). The karst morphology of the Mușeteica glacial valley was preliminarily investigated by Mihai and Moldoveanu (2006). These karst landforms developed under particularly high-alpine climate conditions, typical for the South Carpathians. Currently, mean annual temperatures are 0.8 °C at Bâlea Lake weather station, located at 2060 m elevation in a north-facing glacial cirque (National Meteorological Administration, 2017), and 2.5 °C on the south-facing ridge crest at ~2400 m (Drăgușin et al., 2019). Average precipitation amount is ~1300 mm/y, and snow cover usually persists from November until June. The marble bedrock is covered by a thin, discontinuous soil layer.

2.1. Lithology, tectonics, and structure

The Mușeteica-Buda area is defined by NE-SW-oriented marble stripes of the Făgăraș terrane in the South Carpathian orogen, comprised of a polymetamorphic sequence of sedimentary

4

origin (Balintoni and Pană, 1993) of late Neoproterozoic-early Paleozoic age (Giuşcă et al., 1977; Kräutner, 1980; Balintoni, 1986; Gheuca, 1988; Pană, 1990; Balintoni et al., 2014). Up to four metamorphic events affected the Făgăraş unit and were recognized in rock structure and texture (Stelea, 1992). The $^{40}Ar/^{39}Ar$ ages obtained by Dallmeyer et al. (1998) fall mostly within the 320-300 Ma range, showing the Variscan metamorphic imprint. The low-grade metamorphism was related to contraction and crustal thickening during the Aptian emplacement of Supragetic Nappes and Maastrichtian overthrust of the Getic-Supragetic nappe stack over the Danubian nappe complex (Iancu et al., 2005, and references therein).

The lithology of the central part of Făgăraş Mts consists of gneiss, micaschists, amphibolitic schists, amphibolites, and marbles. The latter are arranged in stripes and lenses ranging from 30 to 250 m in thickness, and up to 5 km in length. The marble sequence hosting the karst of Muşeteica is the thickest (850 m) and longest of all (10 km). It consists of dolomite and calcite across a perpendicular NW-SE transect. The caves formed exclusively in calcite marbles, rich in quartz (0.72% to 18.57%) and micas (C. Marin, pers. comm.). Orientation of the stress field during metamorphism determined a banded texture of marbles, similar to the general structural assemblage of the Făgăraş terrane. The average dip of foliation planes ranges between 30º and 45º, locally exceeding 50º. It corresponds to the S_2 foliation, which is the major structural feature of the entire polymetamorphic sequence of the Făgăraş Unit (Stelea, 1992).

Faults and related fracture systems generally fall within two major structural sets, oriented NE-SW, and NW-SE, respectively. The first set could be attributed to Late Cretaceous to Early Burdigalian transtension-extension and the clockwise rotation of the South Carpathians (Maţenco et al., 1997; Schmid et al., 1998), whereas orientation of the second set suggests the effect of strike-slip movements during the Sarmatian tectogenetic events (Gheuca, 1988; Maţenco and Schmid, 1999).
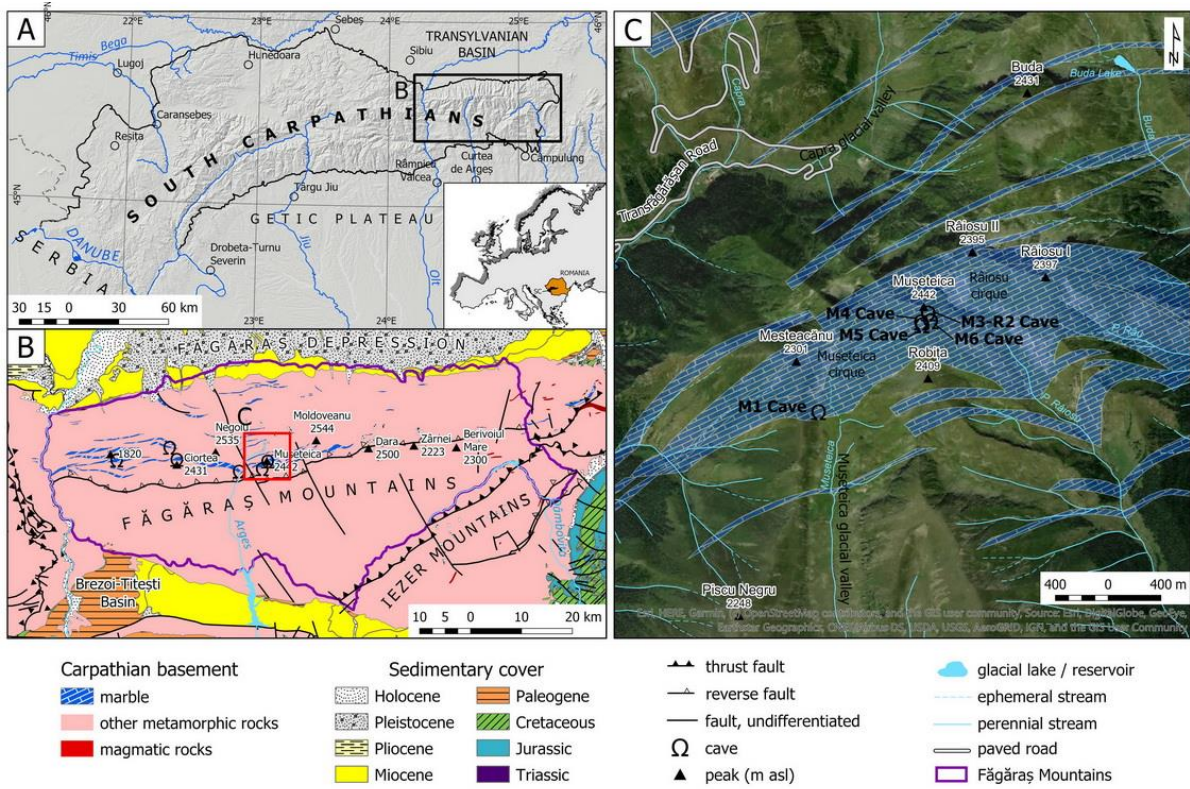
Figure 1. A. Geographic setting of the Făgăraş Mountains (terrain map created from SRTM3 data, courtesy of USGS); Inset showing the location of the South Carpathians (SC) in Europe; B. Geological map of the Făgăraş Mountains modified from Dessila-Codarcea et al. (1968) and location of marble caves (Silvăşanu, 1982; Giurgiu, 1990; Drăguşin et al., 2019); C. Geological and topographic setting of Muşeteica marble karst in the Făgăraş Mountains – modified from Schuster (1977); CNES/Airbus satellite image courtesy of Environmental Systems Research Institute (ESRI)   (2-column fitting image)

2.2. Cave setting

The Făgăraş Mountains host several small caves developed in marbles at elevations of 1200 m (five caves in the Capra Valley at Piscu Negru), and 2080-2430 m (one cave near Budislavu

6

Lake, five caves in the Ciortea Mt, and six caves in the Muşeteica Mt). To the east, four caves developed in the Prislop-Coţi area, at 1500-1600 m (Silvăşanu, 1982).

The presence of ridge-top caves and cave remnants on the Muşeteica-Râiosu crest is a typical feature of glaciokarst landscapes (Smart, 2004). M1 Cave is a former ponor (Giurgiu, 2006) developed in the glacial cirque bottom at ~2100 m, whilst M3-R2, M4, and M5 caves are found on the ridge top, at 2400-2430 m a.s.l. (Fig. 2). One of the collapse dolines (D2) is an unroofed cave remnant, a former passage infilled with sediments (M6 Cave). All the ridge-top caves and dolines are clustered within a 5540-sqm area of triangular shape. They all host flowstones and stalagmites, some of which were progressively exposed by slope retreat. In contrast, speleothems are absent in M1 Cave.
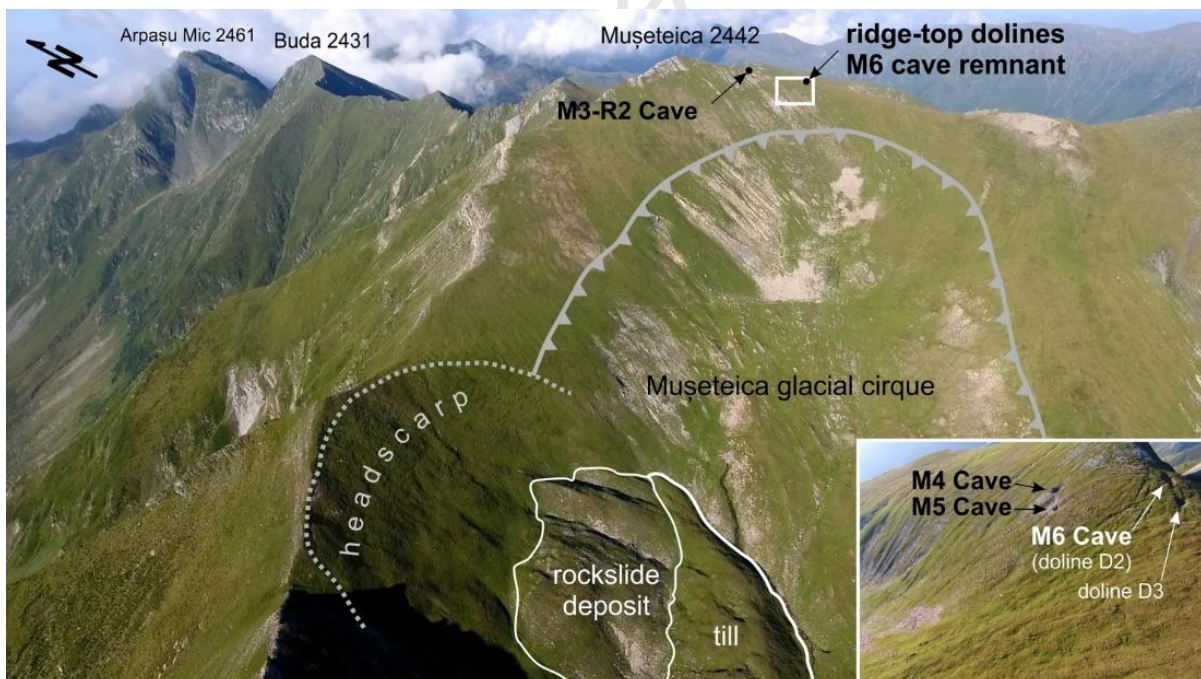

Figure 2. Location of ridge-top caves and dolines (cave remnants) in the Muşeteica area on the UAV oblique aerial photograph. Elevation of summits (m a.s.l.) are given in meters. The white rectangle is about 30 m in width, and the dolines in the inset are ~7 m in width.

(2-column fitting image)

7

3. METHODOLOGY

3.1. Aerial photogrammetry

We surveyed a 1-km^2 area of the Muşeteica glacial cirque using a DJI Phantom4 unmanned aerial vehicle (UAV). A total of 1,314 aerial images were collected at a speed of 5 m/s, with a vertical angle of 90°, and a side and forward overlap of 70%. To increase the horizontal and vertical accuracy, four ground control points were positioned using a Trimble GeoXH 2008 DGPS. The root mean square error for all the points was 0.21 m. A high-resolution digital surface model (DSM) and digital elevation model (DEM) of 50 cm/pixel, and an orthoimage of 10 cm/pixel were generated by using the Drone2Map™ software.

3.2. Geomorphological mapping and morphometry

A detailed geomorphological map was created on a 1:5,000 scale to identify different genetic types of landforms: structural, petrographic, glacial, periglacial, and gravitational. Contour lines were automatically generated from the DSM at different scales to match the mapping purpose. The 5-m contour interval served as a mapping support of all other geomorphic features on the 1:5,000 scale.

The glacial morphometry of Muşeteica cirque was used in order to determine data on the average glacial erosion rate during the Last Glacial Period, the event which left the only physical markers with this respect. In the lack of other evidence, we presumed that the cirque started forming at the beginning of MIS 4 (~70 ka). Five topographic transects were extracted across the cirque, perpendicular to its longest axis at approximately equal intervals, and used to calculate the height range. The cirque height (H) is the difference between the lowest

8

(H_{min}) and the highest (H_{max}) altitude within a glacial cirque (e.g., Federici and Spagnolo, 2004). We calculated the cirque height as the maximum difference in altitude on each profile, then we used the average of these values and the time lapse between the beginning and the end of the Last Glacial Period (LGP) to estimate the maximum glacial erosion rate (E_g) within the cirque, according to the formula below.

$$E_g = \left(\frac{1}{n} \sum_{i=1}^{n} H_i \right) \frac{1}{T} ,$$

where *n* is the number of calculated height range values (here, *n*=5), H_i is the value of each calculated item (i.e., the cirque height), and *T* is the estimated LGP time lapse. The duration of the LGP was estimated at ~59 ka, according to Lisiecki and Raymo's (2005) MIS 5-4 age boundary of ~71 ka, and the deglaciation age for the Făgăraș Mountains of ~12 ka provided by Kuhlemann et al. (2013). The maximum glacial erosion rate is assumed to have occurred along the lowermost points on the cirque floor, and gradually decreased up the headwall towards the crest.

3.3. Structural measurements and orientation analysis

We performed a comparative orientation analysis of cave passages and structural features (joints, faults and fractures). Results were plotted on rose diagrams with a bin width of 10° and on equal-area projection spheres on Schmidt stereonet.

Three sites ranging in size from 50 to 100 m^2 were selected for microtectonic measurements on marble outcrops in the vicinity of caves. We sampled 50─60 joints/site and measured the joint azimuth and dip. The best fit great circles of joint families were compared to stereographic projections of cave passages in order to compare each joint family with cave conduit data.

9

Fault and fracture sets were digitized from various sources at different scales, and plotted against each other on rose diagrams (half circles) to explore the regional and local controls of structural assemblages on cave development. Over 500 fault and fracture segments were extracted in the central Făgăraş Mts from CNES/Airbus satellite images (courtesy of Digital Globe). Documented faults (Dessila-Codarcea et al., 1968; Schuster, 1977) were plotted against the manually-extracted fault set. A supplemental set of fractures and fault segments was extracted from the high-resolution DSM of Muşeteica glacial cirque, and compared to those mentioned above.

Orientation data of underground and surface karst features were either collected during field survey or extracted from the DSM. Cave passages, ridge-top dolines, and shaft entrances were analyzed together, to better constrain the cave system's structural arrangement. The lengths of cave passages rather than frequencies were considered meaningful for analysis, allowing for better highlighting the cave development on preferential orientations.

3.4. Cave morphology

We surveyed the M1, M3-R2, M4, and M5 caves using a modified Leica™ Disto X310 range finder. The processed data were used to extract segments of cave passages, and calculate their morphometry and orientations. We then calculated the pattern morphometric indices (Table 1), synthesized by Piccini (2011), suitable for characterizing the geometry and morphometry of short alpine caves typical to stripe karst (Lauritzen, 2001). The focus was placed on indices' reliability for highlighting the most important morphometric features of a cave, and that they should be selected according to cave geometric properties and spatial complexity (Piccini, 2011). We therefore avoided to use indices that would be better fit for maze or horizontal caves.

10

Table 1. Morphometric parameters and indices calculated for Muşeteica caves

No.	Parameter	Abbr.	Description/Formula (from Piccini, 2011)
1	Real length	Lr	Real development of the cave, cumulating all the passages, including branches and pits.
2	Plan length	Lp	Total length of the plan view of all the cave passages.
3	Vertical range	Rv	Sum of negative and positive drops.
4	Extension	Ex	Horizontal distance of the most far-away points of the cave.
5	Verticality index	Vi	Rv/Lr
6	Horizontality index	Hi	Lp/Lr
7	Linearity index	Li	$(Ex^2-Rv^2)^{1/2}/Lr$
8	Horizontal complexity index	Hci	Lp/Ex

The length of M3-R2 Cave was conventionally calculated as the sum of all its passage segments (n=10), although the lengths of ridge-top branches (n=3), accessible only via the D1 collapse doline (Fig. 6), were not initially added (Tîrlă et al., 2016). However, for analytical purposes these branches will be considered in this study and their lengths cumulated to that of the cave itself. Vertical range coincides with negative drop, since no cave in the Muşeteica system has positive altitude difference.

Cave morphology was analyzed in relation to the three main genetic groups of erosive features and deposits considered relevant for cave development: erosive, chemical, and breakdown forms (Ballesteros et al., 2015). These were illustrated on the geomorphological maps scale 1:300.

3.5. Speleothem U-Th dating and stable isotope analysis

11

Three flowstone samples and a stalagmite were collected from M3-R2, M5 and M6 caves for U-Th dating. Stalagmite M3-R2-1 was collected from the main chamber of the M3-R2 Cave, at 15 m from the entrance. It is 5-cm long and composed of densely compacted, white translucent calcite and presents a thin outer clayey crust. Seven samples for U-Th dating, averaging 100 mg, have been hand drilled at equal intervals along the growth axis and measured at CENIEH (Burgos, Spain). A total of 197 samples were micro-milled along the growth axis and their stable isotope composition ($\delta^{13}C$ and $\delta^{18}O$) was measured on a Thermo Delta V Advantage mass spectrometer coupled with a Kiel IV carbonate device, at the University of Oxford.

Flowstone M3-R2-3 was collected from the middle of the main chamber of M3-R2 Cave. Its basal 3 cm are composed of dark brown calcite with two thin moonmilk layers and two clayey detrital layers. The next 1.7 cm are composed of lighter, more amorphous calcite with distinct light brown lamina and is finally followed by 1.2 cm of moonmilk. Four U-Th sub-samples were hand-drilled: one from the base, two bracketing the petrographic transition at 3 cm and one from the top of the second section, just below a thick moonmilk layer that forms its top.

Flowstone M5-1 is 13-cm thick and composed of a succession of light and dark calcite, with two thin moonmilk layers in its upper part. Several oxide-rich layers can also be distinguished in the section. Three U-Th samples were retrieved from base, top, and above a transition from light to brown calcite, at 8 cm from the base.

Flowstone M6-1 (Fig. 3B) was collected from the western wall of the M6 collapse doline, after the excavation of ~1 m of infilling material. Two U-Th samples were taken from its base and top.

All flowstone U-Th samples were prepared and analyzed at the Max Planck Institute for Evolutionary Anthropology (Leipzig, Germany) following the procedures of Hoffmann et al.

(2007) and Hoffmann (2008), and at the University of Melbourne (Australia) according to the procedure of Hellstrom (2003).

Samples for low resolution isotope profiles were hand-drilled at 5 mm distance for M3-R2-3 (n=12) and M5-1 (n=27). Powder samples were also taken by hand drilling from three host rock samples from near the ridge-top caves, labeled M5-3, M3-R2-1, and M3-R2-2 (should not be confused with speleothem labeling). They were analyzed at Northumbria University, using a Thermo Delta V Advantage coupled with a GasBench II sample preparation device.

3.6. Sediment infill of doline D2 – stratigraphy, ^{14}C dating and pollen content

The clastic sediment infill of the D2 doline was excavated to a depth of ~2 meters, without reaching the bottom. Stratigraphy was described based on field observations. Bulk samples were taken at 10-cm intervals, on thicknesses of around 2-4 cm, and kept refrigerated in plastic bags. Grain size content of seven global samples was analyzed at the Geotechnics Laboratory of the University of Bucharest, following the standard procedure STAS 1913/5-85. First the samples were weighed and introduced into the oven at 105°C for 24 hours, to remove the organic matter. water and lithium carbonate were added in the dry samples and left for 24h, then the cement was separated using the 0.063 mm sieve. The mass of the cement resulting from washing exceeded 10% of the sample and was further analyzed by applying the sedimentation and Sieve-pipette methods for the fine fractions and sieving only for the coarse fractions (Gee and Bauder, 1986). Based on the data obtained, particle size and percentage were determined for each of the following Udden-Wentworth classes: a) larger than 2 mm; 2-0.063 mm; c) 0.063-0.004 mm; d) smaller than 0.004 mm (Wentworth, 1922).

Three samples for optically stimulated luminescence dating were taken by hammering a 20 cm long plastic tube into the sediment and were analyzed at the Babes-Bolyai University in

Cluj-Napoca, Romania. No age estimation could be obtained, possibly due to a very young age of the deposition (A. Gabor, pers. comm.).

Following the indication of a very young age and in order to obtain a preliminary chronology for the sediment infill, we performed radiocarbon measurements on three bulk samples (M6-4, M6-10, and M6-19) taken from depths of 37-40 cm, 98-100 cm, and 188-192 cm respectively. Samples were prepared and measured at the Horia Hulubei National Institute for Physics and Nuclear Engineering (RoAMS) in Măgurele, Romania, following the procedures described in Sava et al. (2018). The samples were first observed under optical microscope to check for the presence of macrofossils (i.e., seeds, twigs, plant remains). Since no macrofossils were identified, we decided to separate the organic carbon fraction by leaching the inorganic carbon from the bulk sample. This operation was done by dissolving the carbonate with 0.5 M HCl during three days of treatment, with ultrapure water rinsing in between the acid steps. At the end of the procedure, the pH was set to neutral adding ultrapure water, followed by sample drying at 60°C. The organic carbon was then collected for the graphitization step. The ^{14}C ages were calibrated using the Oxcal online program (Bronk Ramsey, 2009), based on the IntCal13 calibration curve of Reimer et al. (2013).

One random 2-cm³ sediment sample (M6-16, from ~140 cm deep) was selected and prepared in order to extract and assess the quality of preservation of pollen and spores, following the procedure described in Moore et al. (1991). Pollen and microspore identifications were made under 400x magnification using the descriptions and identification keys in Moore et al. (1991) and Beug (2004), and by comparison to reference collections.

4. RESULTS

4.1. Glaciokarst landforms

14

4.1.1. Alpine karst

Apart from caves, the most common karst landforms are dolines, karren, ponors, and dry valleys. Three dolines (D1-D3) lined up on the NNW-SSE-oriented fracture that dissects the Muşeteica Mt. formed by the collapse of cave passages, thus being genetically different from the rest of twenty-two dolines (Fig. 4A). These dolines formed by dissolution, and twelve formed partially by the subsidence of glacial till. Such dolines are typical to covered karst morphology (Veress, 2016). Their position indicates a possible origin of subglacial streamflow subsapping, the cuvettes evolving into dolines during postglacial dissolution. Seven additional dolines have developed by dissolution, atop or amongst the roches moutonnées. The largest solution doline (D20, Fig. 4F) preserves a functional ponor and suggests that an important karst conduit developed underground, to the north of M1 Cave, on the same N-S direction. Both doline D20 and M1 Cave close the valley line right above the plucking slope face which marks the threshold between the cirque and the glacial valley. Karren are best developed on the western-facing side of the glacial cirque, cutting perpendicularly on foliation, on the lee sides of roches moutonnées (Fig. 4G).
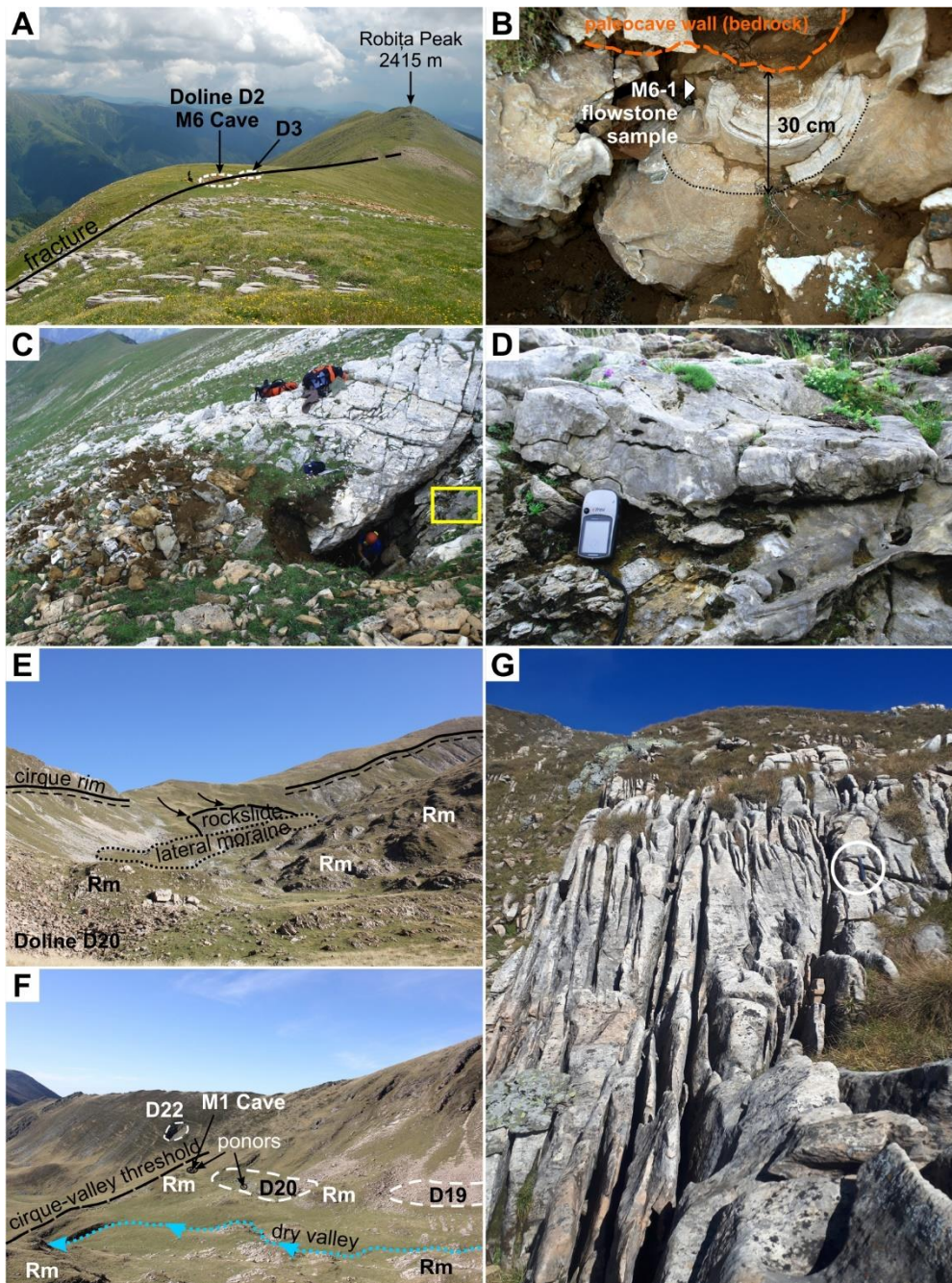
Figure 3. Karst and glacial landforms with cave deposits in the Mușeteica area. A. Ridge-top dolines and M6 Cave; B. Stalactites and flowstones discovered in the unroofed M6 Cave; C. The entrance of M5 Cave, yellow square indicates the extent of flowstone in Fig. 3D; D. Exposed flowstones near M5 Cave (GPS receiver is 10 cm in length); E, F. Glaciokarst landforms in the Mușeteica cirque (Dn – dolines; Rm – roches moutonnées); G. Kluftkarren formed on roches moutonnées (the size of rock hammer is 40 cm). (1.5-column fitting image)

16

4.1.2. Glacial and periglacial landforms

Inherited glacial features include the Mușeteica cirque, the Mesteacănu, Robiţa, Mușeteica, and Râiosu pyramidal peaks, and the interconnecting crests. Mușeteica and Râiosu glacial cirques developed entirely on marbles. The boundary between the cirque and the glacial valley consists in a 15-meters high plucking slope face, which matches the lithologic contact between marbles and the more friable actinolite schists.

Morphometric parameters of the Mușeteica glacial cirque reflect a pronounced allometry, which is typical for the cirques of the Făgăraş Mountains (Mîndrescu and Evans, 2014): 1 km in length, 524 m in width, and an amplitude of 280 m, resulting a length/width ratio of 1.9. The height range is 2100 to 2380 m, and the headwall height is 120 m. It is a valley-head cirque with an area of 0.49 km^2, comparably larger than the Râiosu cirque to the east (0.12 km^2), and the small, nested cirques (0.02-0.08 km^2) hanging on the western and northern slopes of Mușeteica Mountain at ~2000 and ~2200 m a.s.l.

The values used for calculating the average glacial erosion rate are given in Table 2. The five topographic profiles across the Mușeteica glacial cirque along which we calculated the cirque height are illustrated in Figure 4.

Table 2. Morphometric parameters of the Mușeteica glacial cirque, calculated from DEM-derived values.   (1-column fitting table)

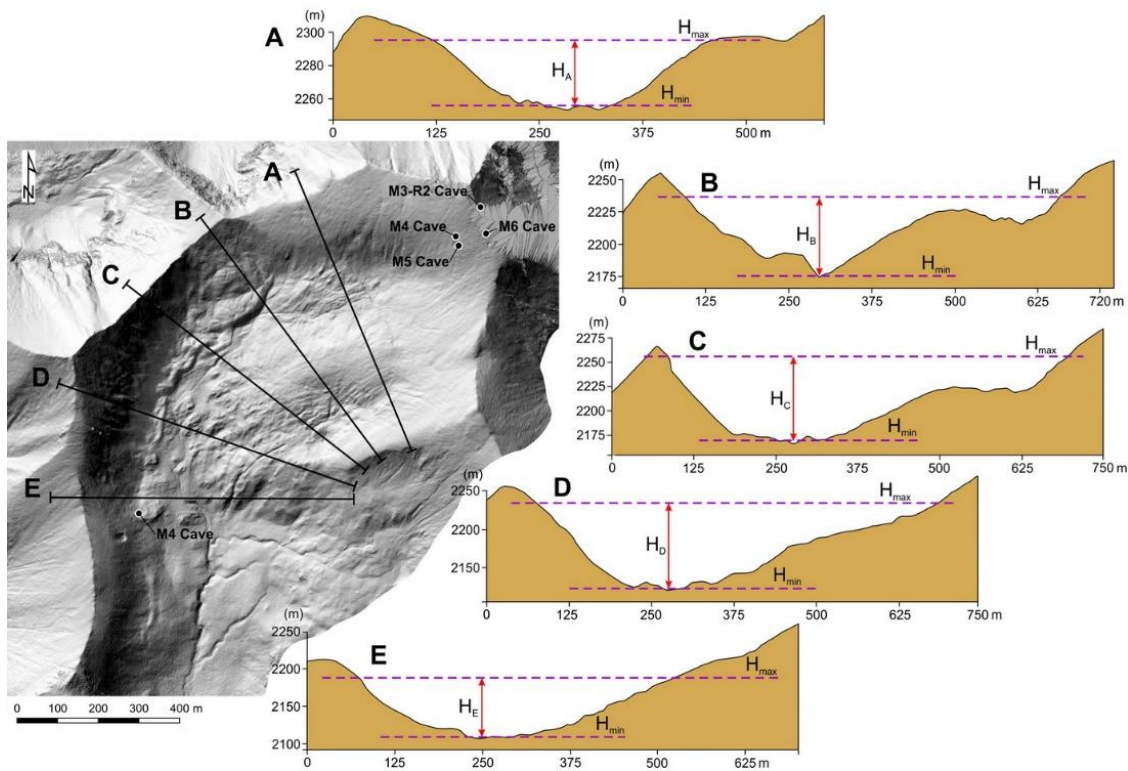| Profile	Max. elevation (m a.s.l.)	Min. elevation (m a.s.l.)	Cirque height (m)
A	2295	2255	40
B	2235	2175	60
C	2240	2154	86
D	2220	2128	92

| E | 2175 | 2094 | 83 |

Figure 4. Topographic profiles across the Mușeteica glacial cirque. Double arrows indicate the cirque height for each profile. (1.5-column fitting image)

The cirque height varies in thickness from 40 m in the vicinity of upper crest to more than 90 m near the threshold, resulting in an average height of 72.2 m.

Roches moutonnées have distinct morphologies in the upper cirque compared to those in the lower cirque. The former features are smaller, more discrete (1-2 meters in height) and generally subsequent to marble foliation. The latter group comprises well-developed features (5-10 m in height), with well-preserved lee side facets due to ice flowing in the same direction as the dip of marble foliation. Glacial till is preserved only on the western side of the cirque bottom. Lateral moraines reach between 5 and 20 meters in height and host subsidence dolines. Avalanche channels are well developed on the steep, eastern-facing side

18

of the cirque headwall. These channels end with imbricated triangular marble scree cones, which partly cover the lateral moraines.

4.1.3. Gravitational landforms

A large, meter-deep mass movement breaks the continuity of the glacial rim to the NW. Field observations show that it is a massive consequent rockslide, seeming to have been driven parallel to the marble foliation dip plane. A rockslide deposit is superimposed on the lateral moraines accumulated on the right side of the cirque bottom. Another distinctive linear feature was observed at the glacial headwall base, striking on a NW-SE direction, perpendicularly to the direction of cirque development. It has a sackung-like morphology, more similar to a smoothed slope break along an inherited fracture. Sackungs (sackungen) are upslope-facing scarps formed in (but not restricted to) glaciated mountains near the ridge crest in postglacial time intervals due to gravitational spreading (e.g., Gutiérrez-Santolalla et al., 2005). In Mușeteica Mt., both gravitationally developed landforms are deep-seated gravitational slope deformations, an evidence of postglacial unloading. These can be observed on the digital surface model as smooth terrain discontinuities.

The geomorphological map of the area that hosts the caves (Mușeteica ridge crest and the cirque from the SW slope) shows the variety of genetic types of landforms which could have influenced the conduit development and cave deposit formation to some extent (Fig. 5). Surface deposits like talus scree, glacial till and rockslide deposits increase the landscape complexity, but these also cover, destruct or hinder surface karst development. Triangular talus scree deposits with angular marble fragments fringe at the base of snow avalanche channels, developed only on the eastern-facing cirque headwall.

The glaciokarst is divided into two areas: a) *the area above the trimline* containing the ridge-top caves and collapse dolines; b) *the relict glacial cirque* with solution and subsidence dolines, ponors, karren-incised roches moutonnées, and dry valleys.
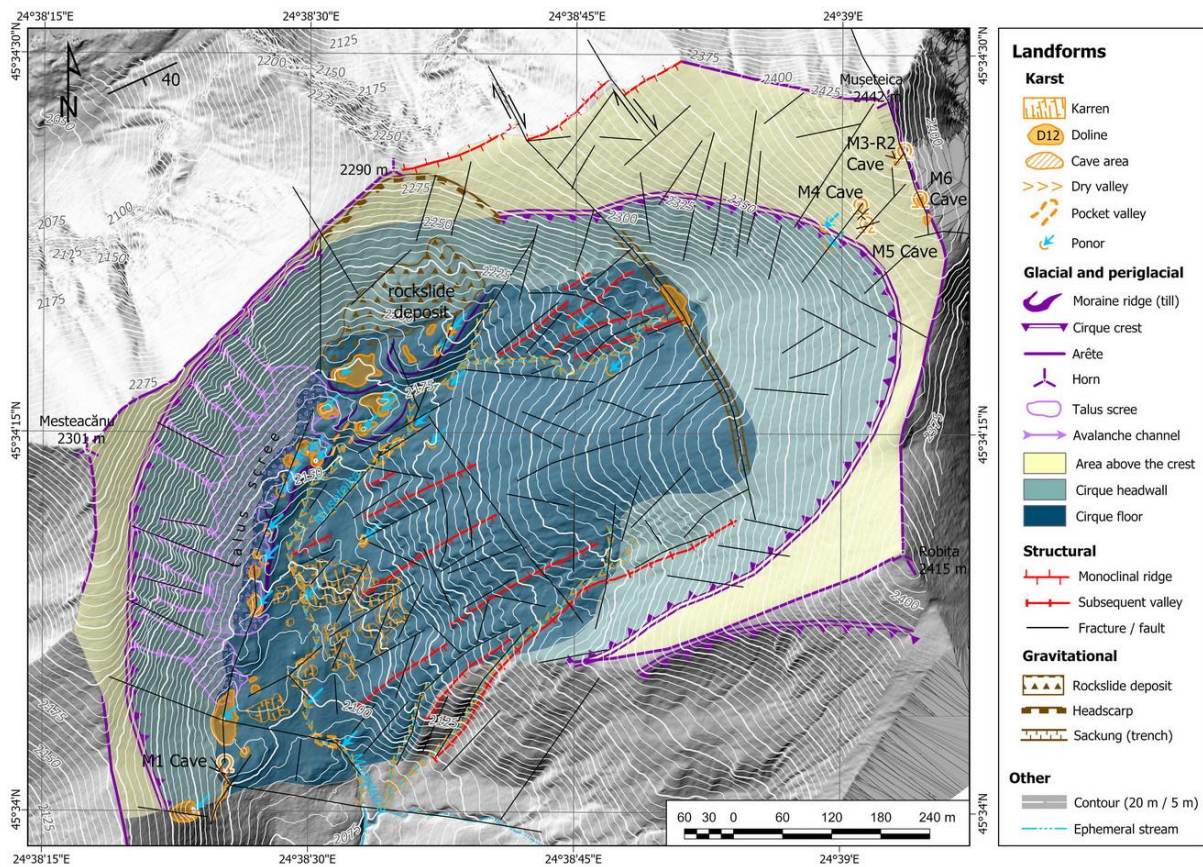
19

Figure 5. Geomorphological map of the Mușeteica glaciokarst (scale 1:5,000). The average strike and dip of marble bedrock is indicated to the upper-left corner of the map. Truncated and unroofed ridge-top caves are shown to the right-up corner.   (2-column fitting image)

4.2. Cave geometry, morphometry and geomorphology

The caves have a single level, are very short and have a simple orthogonal pattern, imposed by the structural control of joint and fault network (Fig. 6). The highest caves (M3-R2, M4, and M5) developed perpendicularly to the marble foliation dip, along a NE-SW direction (40-50°). Only the upper part of the M3-R2 Cave, the M6 unroofed cave and the ridge-crest collapse dolines are oriented NNW-SSE, conformably to foliation dip. Cave passages usually developed along fractures and were widened along foliation planes.

20

M1 Cave developed preferentially at the contact between marbles and an amphibolite stripe (more easily weathered), with subsequent thin actinolite- and biotite-rich sheets interlayered within the marble. The cave has the steepest profile of all the caves in the area, about 45-53° on the foliation planes and 70-90° on the fault cross-cuts (Fig. 7). It is nearly a subvertical cave with limited development, a feature which is typical for stripe karst (Lauritzen, 2001). In the first section, large chambers are filled with breakdown deposits, which often form the walls and even ceiling of adjoining passages. The walls of the primary tube, covered by scallops, were only partially preserved. A very low and narrow tube (W=1 m, H=0.3 m) links the upper chambers to the lower passage of the deepest section (Fig. 8). This last passage also has a tube morphology with an ellipsoidal profile evidencing the structural control of foliation planes upon the cave passage enlargement under pressure flow. Consequently, the passage is very wide (~7 m) compared to its height (0.3 to 1 m) and no breakdown evidence was observed along this part. Overall, tube morphology is pervasive in the M1 Cave, except for the frontal part, recently collapsed and filled with breakdown. Unlike the ridge-top caves, where they are abundant, speleothems are absent in the M1 Cave, indicating different environmental conditions which inhibited their growth.

M3-R2 Cave is very wide and deep, in contrast to its shortness (Table 2), showing a preferential development along the marble foliation plane. A detailed description was made by Tîrlă et al. (2016). Its main passages intersect at 90º angle and are separated only by breakdown walls. The passage ends with a large breakdown blocks accumulation, which may indicate a possible continuation. The morphology and orientation of exposed cave remnants are somehow different, controlled by the NW-SE fracture that crosses through the Muşeteica north-western nested cirques and the ridge crest.

M4 and M5 are truncated caves located next to each other (~15 m apart), and very close to M3-R2 Cave. M4 Cave (25 m in length) is filled with breakdown, mostly unstable, preserving only a thin (1-2 cm) flowstone fragment on the outer wall, at the base of the

entrance. M5 is the shortest remnant cave (16 m in length) consisting in a simple passage opened upwards through a 2.7-m shaft. Flowstone sample M5-1 was retrieved just outside the cave entrance – indicating a past larger extent of this cave, since speleothems of this kind could have formed only underground.

M6 is an unroofed cave passage found after excavating into the D2 ridge-top doline. The doline is filled with more than 2 meters of sediment and seems to continue with a small passage, although exploration work is still needed to access it. The walls at the western end host well-preserved speleothems, while many speleothem fragments can also be found within the clastic infill.

Morphometric indices are typical for alpine small caves (e.g., Piccini, 2011) and have comparable values influenced mostly by the geological conditions (Table 3).

Table 3. Morphometric parameters and indices of Mușeteica marble caves. Dimension values are given in meters and angles in degrees.

| Cave name	Geographic coordinates	Elevation (m asl)	No. of passage segments	Lr	Lp	Rv	Ex	Vi	Hi	Li	Hci	Strike	Dip
M1**	45°34'0.68"N 24°38'19.63"E	2106	15	132	104	-70.6	85.4	0.53	0.78	0.36	1.22	18.3	43
M3-R2*	45°34'25.11"N 24°38'57.69"E	2430	13	55	48	-18.2	25	0.36	0.87	0.11	1.92	40	45
M4**	45°34'22.95"N 24°38'55.56"E	2401	4	25	14	-11.5	23.5	0.46	0.56	0.15	0.90	37	45
M5**	45°34'22.18"N 24°38'55.75"E	2396	5	16	14	-3.7	11.3	0.23	0.88	0.08	1.24	52	42
M6**	45°34'23.15"N 24°38'58.79"E	2417	1	13	13	5?	13	-	-	-	-	152	-

*Tîrlă et al., 2016; **This study
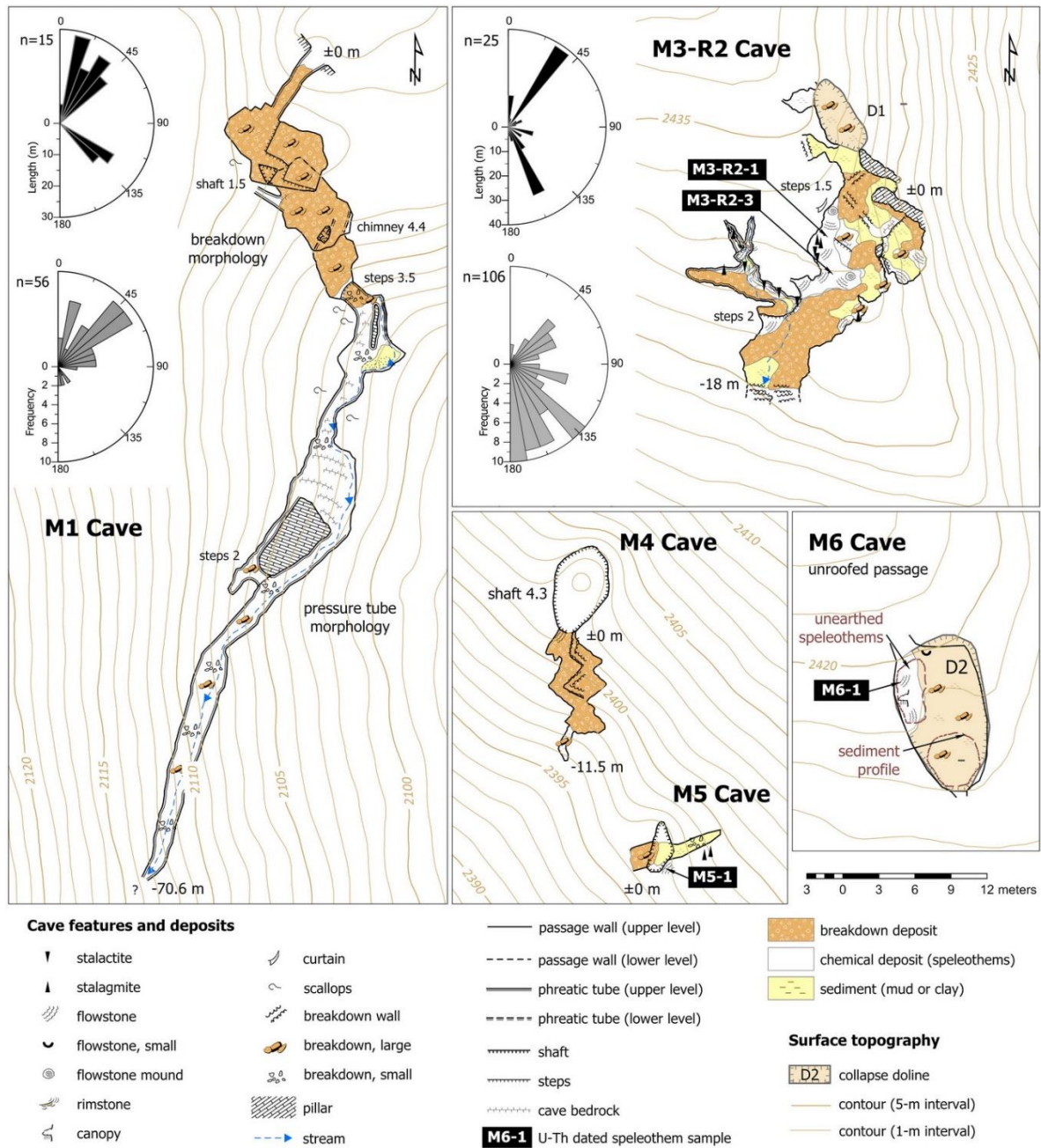
Figure 6. The geomorphological map of the Mușeteica caves and cave remnants. Arrows indicate speleothem sampling sites (sample names in black framed text). Sample M3-R2-1 was analyzed and discussed by Drăgușin (2013). Rose diagrams show orientations of passage ways (black arrays) and joint sets (grey) for each site.   (2-column fitting image)
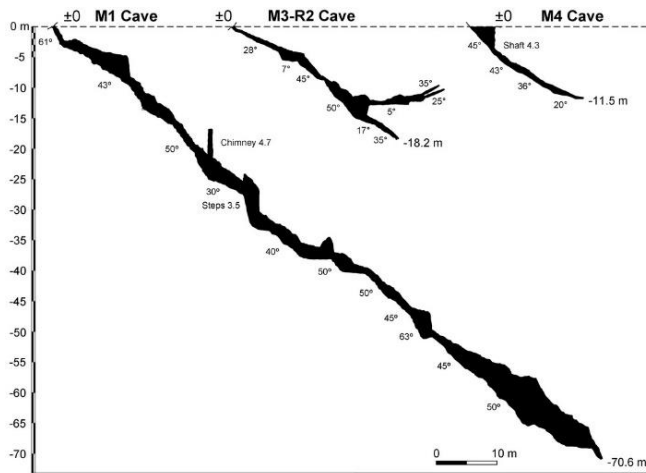
Figure 7. Unfolded longitudinal profiles of the M1, M3-R2 and M4 caves. Passage inclination is displayed below the profiles, and cave depth at the ends.   (1-column fitting image)

The highest contrast is shown by the value of *Li*, which is much higher for M1 Cave than for the ridge-top caves (0.36 vs >0.15, respectively). *Hi* should be similar considering the dip of the main passages (42-45º), which is conformable to the dip of marble foliation. However, the *Hi* value of M3-R2 Cave is high (0.87) due to low-dipping branches and upper passages. The cave has the highest *Hci* (1.92) and a low *Li* (0.11) due to its complex areal development, which could be an evidence of a formerly longer conduit network.

24
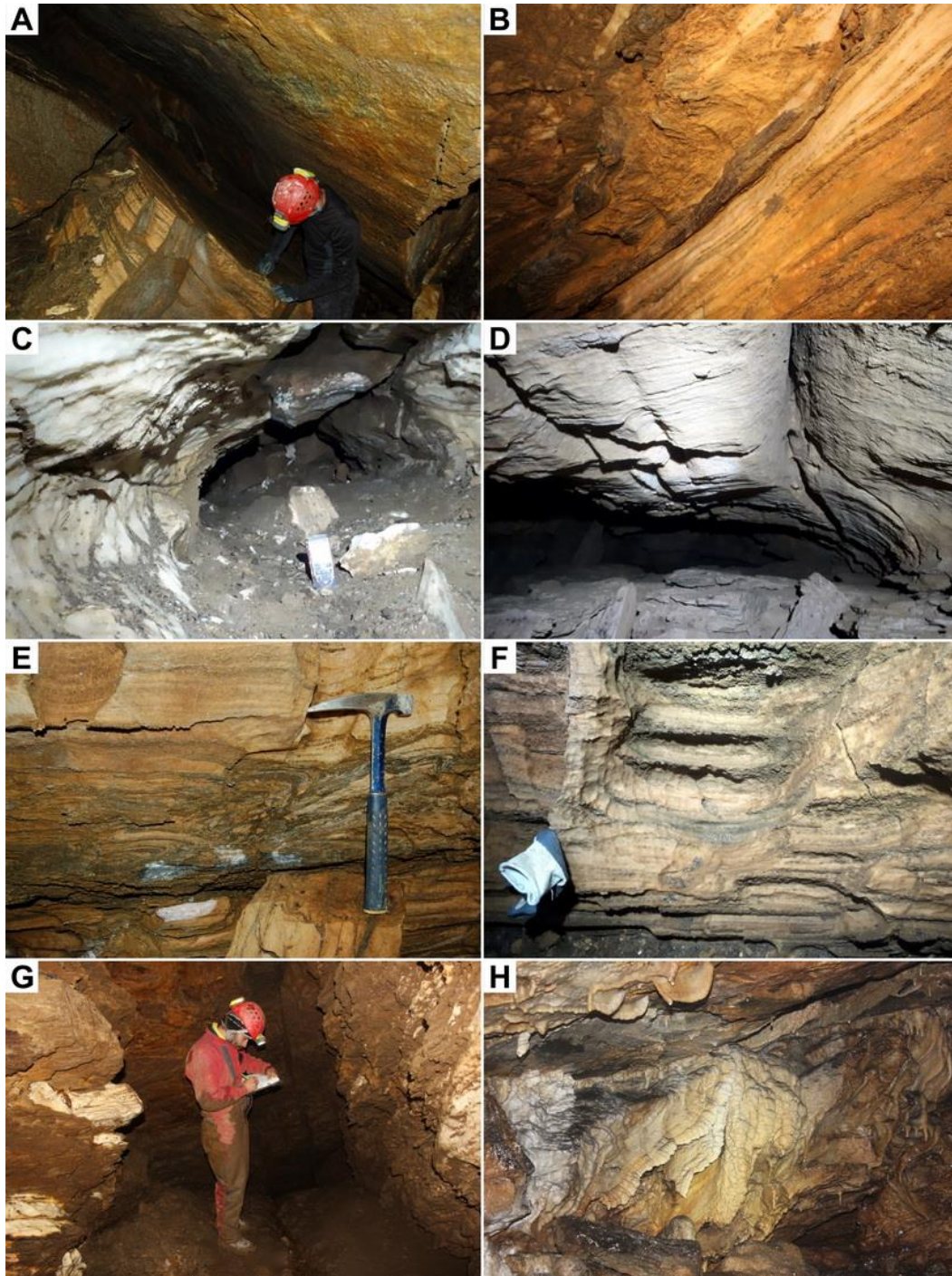
Figure 8. Morphological features of the M1 (A-G) and M3-R2 caves (H). A. Passage ways developed along foliation planes; B. Weakness planes along the marbles - amphibolitic schists contact; C-D. Pressure tube morphology; E-F. Wall and ceiling pockets formed in the frontal cave sector by late-stage condensation corrosion due to invasion of warm air during the summer season; G. The lowermost point of M1 Cave (-70 m); H. Speleothem decorations in M3-R2 Cave.　　　(1.5-column fitting image)

25

4.3. Orientations of structural and karst features

4.3.1. Fault and fracture system

Three main orientations of the major faults were distinguished: NW-SE, W-E, and NE-SW (Table 4). With small differences, this pattern matches orientations of the medium-scale fault and fracture set extracted from the CNES/Airbus imagery (Fig. 9A).

The NE-SW and N-S oriented fractures are the most frequent, in contrast to the regional tectonic system. Several NNW-SSE-oriented faults and fractures cross the upper part of the Mușeteica glacial cirque and the Mușeteica-Robița ridge. The latter partially controlled the development of the M3-R2 Cave and the passages which were subsequently unroofed and infilled with sediments (e.g., M6 Cave). This major fracture crosses the Mușeteica Peak and is visible on the NW-facing slope. Recent dissolution and collapse occurred along it between the M3-R2 and M6 caves, where it intersects the main fracture of M4 Cave (Fig. 9B). Two NW-SE oriented main fractures cross the upper part of the glacial cirque transversally. The easternmost one forms the boundary between the cirque floor and the headwall, and favored the opening of a shallow trench of 0.5-1 m in depth (Fig. 5).

The preferred orientations for development of underground karst conduits in the Mușeteica area were NE-SW and NW-SE. The two passage sets normally intersect under 90º angles, forming orthogonal networks. Cave passages having a cumulative length of 114 m out of a total of 236 m are NE-SW oriented, while those oriented NW-SE are 55 m in length. The WNW-ESE and NNE-SSW passages sum 22 m and 18 m, respectively.

Table 4. Main orientations of joints, faults, fractures, and cave passages

Structural / karst features (lettered a-e in Fig. 9D)	Sample size	Orientations
a. Major faults (Făgăraș Mts)	36	NE-SW, W-E, NW-SE
b. Faults and fractures (Făgăraș Mts)	540	NE-SW to ENE-WSW, and WNW-

26

		ESE to NW-SE
c. Local faults and fractures (Muşeteica cirque)	137	NE-SW, NW-SE, WNW-ESE
d. Local joint sets, cumulated (Muşeteica caves)	162	NE-SW, NNE-SSW, NW-SE
e. Cave passages (length distribution)	40	NE-SW, NW-SE
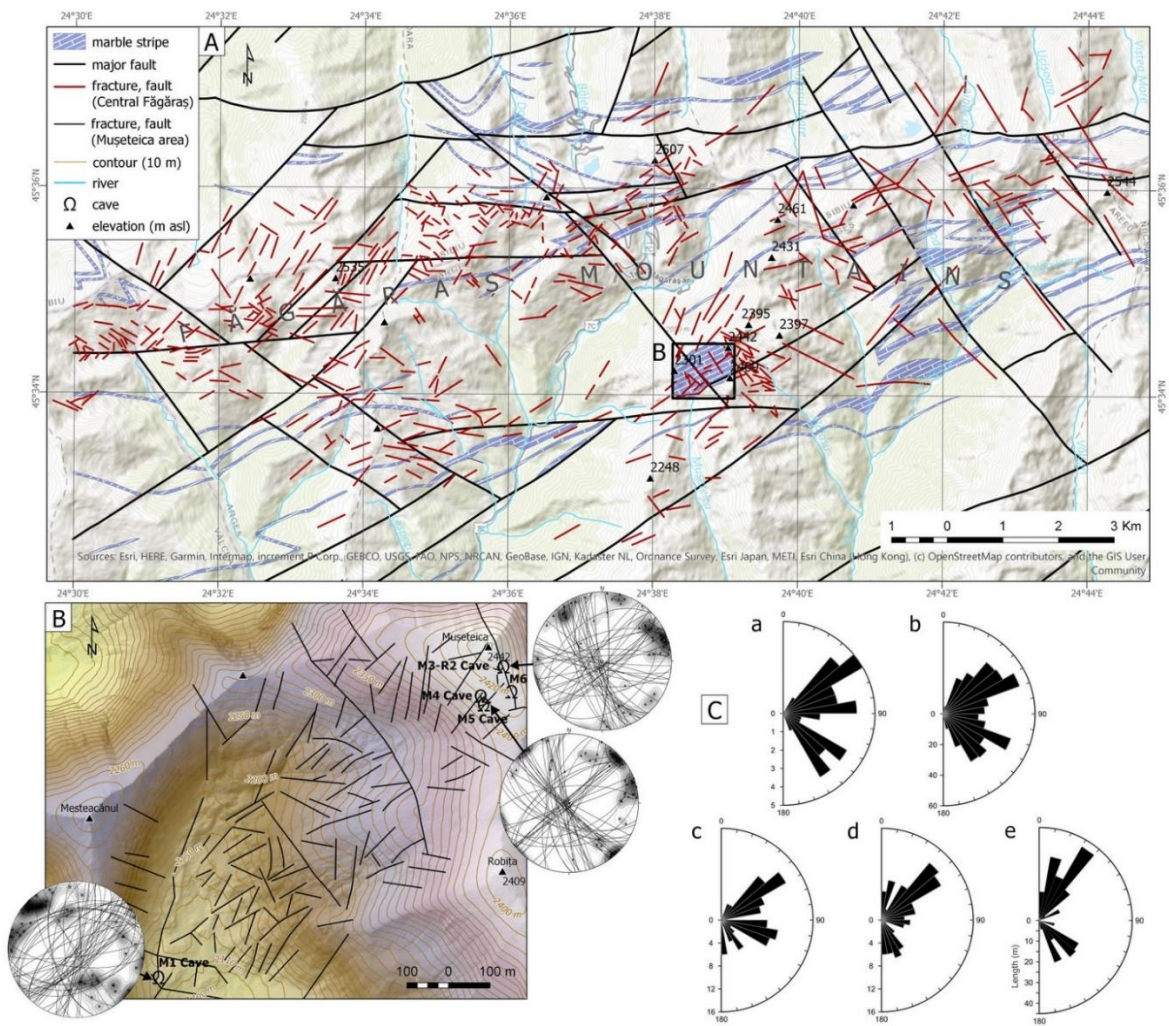
Figure 9. Structural framework of the central Făgăraş Mountains (A), and Muşeteica cirque (B). Orientation rose diagrams of faults, fractures, joints, and cave passages (C). Data source: A. Documented major faults and fault segments extracted from medium-resolution DEM (courtesy of Digital Globe); C. Large-scale fault segments and fractures extracted from high-resolution DSM (hillshade); D. Explanation of letters (a-e) in Table 3. (2-column fitting image)

27

4.3.2. Types of joints and the joint families

The joints generally form two systematic sets forming an orthogonal network (Fig. 9B), close-fitting a tension joint system (Passchier and Trouw, 2005). Shear joints form conjugate sets that intersect the former under a sharp angle (30-60º). This pattern is better observed on the ridge, near the entrance of M3-R2 Cave. Frost-weathering joints developed on preferred detachment planes of the minerals and have sub-decimetric to sub-centimetric densities. They distinguishable by their high density compared to that of schistosity and shear joints, the latter being strictly controlled by tectonics. The joint sets measured near the caves fall into four families (Fig. 10), of which only one (J1) seems to be common to the entire study area. Another three joint groups were identified, two on the ridge-top (J2, J3) and one on the valley bottom (J4). Results show that the J1 joint family is responsible for the development of Muşeteica caves. The main passages of M1, M3-R2, M4, and M5 caves developed along NW-SE-oriented joints and fractures.
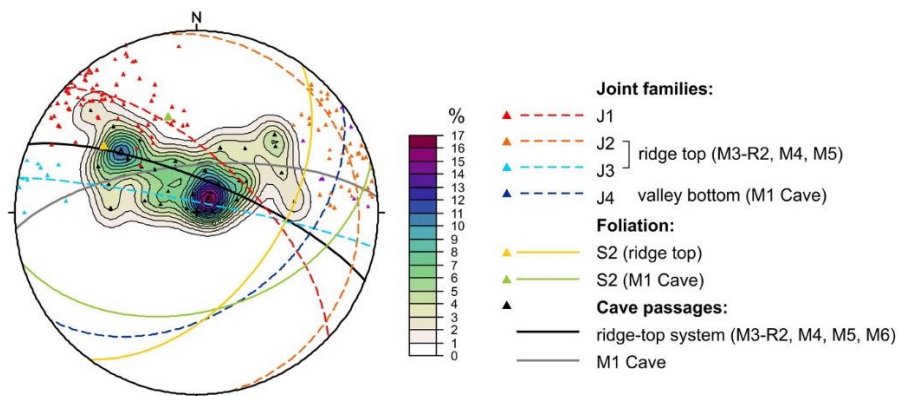

Figure 10. Stereograms of joint and foliation planes combined with cave passages (best-fit great circles and poles to planes). Contour levels show the density of points representing polar projections of cave passages.   (1.5-column fitting image)

4.4. Speleothem U-Th ages

Results of U-Th dating are given in Table 5 and plotted in Figure 11. A low concentration of uranium can be seen across all sub-samples of the four speleothems, with an average value below 20 ng/g, a maximum of ~50 ng/g (sample M6-1) and a minimum of ~10 ng/g (sample M3-R2-3). Stalagmite M3-R2-1 seems to have formed during a short, 2000-year period, roughly between 125 ka and 123 ka.

Flowstone M3-R2-3 has a base age of 329.8±11.1 ka and a top age of 97.6±26.6 ka. The middle samples taken across the petrographic transition at 3 cm are within the error bars of each other. The base and top ages of the M5-1 flowstone are 440.2±36.8 ka and 398.8±29.8 ka, respectively, with high uncertainties, of about 8%. The sample in the middle returned a 31% uncertainty (542.9±168.7 ka), being nevertheless within the uncertainty of the other two. The base age of M6-1 flowstone is older than 560 ka, beyond the limit of U-Th dating method, and its top age is 526 (+97/-52) ka.

Table 4. Results of the U-Th measurements. Letters [a], [b], and [c] in the column *Sample ID* indicate the place of analysis: [a] - CENIEH, Burgos, Spain, [b] - University of Melbourne, Australia and [c] - Max Planck Institute for Evolutionary Anthropology, Leipzig, Germany. Age uncertainties are reported at 2σ confidence interval.

Sample ID	^{238}U (ng/g)	^{232}Th (ng/g)	$[^{230}Th/$ $^{232}Th]$	$(^{232}Th/^{238}U)$	$(^{230}Th/^{238}U)$	$(^{234}U/^{238}U)$	age (ka)	$(^{230}Th/^{238}U)$ corrected	$(^{234}U/^{238}U)$ corrected	Corrected age (ka)	$(^{234}U/^{238}U)$ initial
[a]M3-R2-1 - I	19.77 ±0.12	0.23 ±0.00	284.96 ±2.54	0.00381 ±0.00004	1.0857 ±0.0075	1.5106 ±0.0055	125.0 ±1.7	1.0860 ±0.0076	1.5122 ±0.0056	**124.9 ±1.7**	1.729 ±0.007
[a]M3-R2-1 - II	20.48 ±0.26	0.29 ±0.00	236.83 ±2.47	0.00466 ±0.00010	1.1052 ±0.0145	1.5155 ±0.0289	128.2 ±5.5	1.1056 ±0.0145	1.5174 ±0.0290	**128.0 ±5.5**	1.743 ±0.032
[a]M3-R2-1	19.80	0.23	285.14	0.00381	1.0871	1.5230	123.4	1.0874	1.5246	**123.2**	1.743

|											
- III	±0.13	±0.01	±3.28	±0.00013	±0.0110	±0.0084	±2.5	±0.0110	±0.0084	**±2.5**	±0.010
[a]M3-R2-1 - IV	19.92 ±0.11	0.24 ±0.00	266.18 ±2.17	0.00397 ±0.00004	1.0574 ±0.0062	1.4787 ±0.0056	124.4 ±1.5	1.0576 ±0.0062	1.4802 ±0.0057	**124.2 ±1.5**	1.682 ±0.007
[a]M3-R2-1 - V	19.14 ±0.10	0.25 ±0.00	250.23 ±2.64	0.00423 ±0.00008	1.0592 ±0.0090	1.4927 ±0.0059	122.6 ±2.0	1.0594 ±0.0090	1.4944 ±0.0060	**122.4 ±2.0**	1.699 ±0.008
[a]M3-R2-1 - VI	18.03 ±0.10	0.22 ±0.00	274.19 ±3.37	0.00402 ±0.00006	1.1023 ±0.0085	1.5204 ±0.0071	126.8 ±2.0	1.1027 ±0.0086	1.5220 ±0.0071	**126.6 ±2.1**	1.747 ±0.009
[a]M3-R2-1 - VII	20.12 ±0.10	1.14 ±0.01	59.33 ±0.46	0.01851 ±0.00015	1.0984 ±0.0067	1.5302 ±0.0059	124.5 ±1.6	1.0999 ±0.0069	1.5382 ±0.0072	**123.6 ±1.7**	1.763 ±0.008
[c]M3-R2-3-I	23.21 ± 0.08	7.78 ±0.03	8.47 ±0.04	0.11009 ±0.00020	0.9299 ±0.0051	1.0674 ±0.0033	212.9 ±4.3	0.9231 ±0.0069	1.0739 ±0.0054	**204.0 ±5.6**	1.131 ±0.009
[c]M3-R2-3-II	11.34 ± 0.04	5.15 ±0.02	6.40 ±0.05	0.14908 ±0.00029	0.9512 ±0.0083	1.0896 ±0.0042	211.3 ±6.2	0.9446 ±0.0105	1.1017 ±0.0088	**199.5 ±8.0**	1.179 ±0.013
[b]M3-R2-3 III	35.70		54.90 ±1.50	0.0207 ±0.0004	1.1383 ±0.0057	1.1464 ±0.0026	329.86 ±11.33			**329.8 ±11.1**	1.3714 ±0.0105
[b]M3-R2-3 IV	9.66 ±0.73	12.81± 1.02	2.30±0.07	0.4327 ±0.0113	0.9788 ± 0.0267	1.3125 ± 0.0088	137.4 ±7.3	0.9789± 0.0268	1.3126±0.0088	**97.4 ±25.9**	1.412 ±0.031
[c]M5-1-I	14.33 ± 0.05	0.59 ±0.00	76.15 ±0.47	0.0135 ±0.00006	1.0245 ±0.0049	1.0310 ±0.0031	441.3 ±36.7	1.0248 ±0.0050	1.0313 ±0.0031	**440.2 ±36.8**	1.109 ±0.009
[c]M5-1-III	14.76 ±0.06	0.34 ±0.00	137.23 ±0.93	0.0076 ±0.00003	1.0386 ±0.0061	1.0484 ±0.0039	399.4 ±29.7	1.0388 ±0.0062	1.0487 ±0.0039	**398.8 ±29.8**	1.150 ±0.010
[b]M6-1-I	23.62		14.9 ±1.50	0.0716 ±0.0014	1.0661 ±0.0081	1.0442 ±0.0038	717.11 ±301.70			**>560.0**	1.3861 ±0.5799
[b]M6-1-II	50.90		59.90 ±1.50	0.0188 ±0.0004	1.1232 ±0.0058	1.0941 ±0.0026	531.31 ±77.04			**526.0 +97/-52**	1.4235 ±0.0951
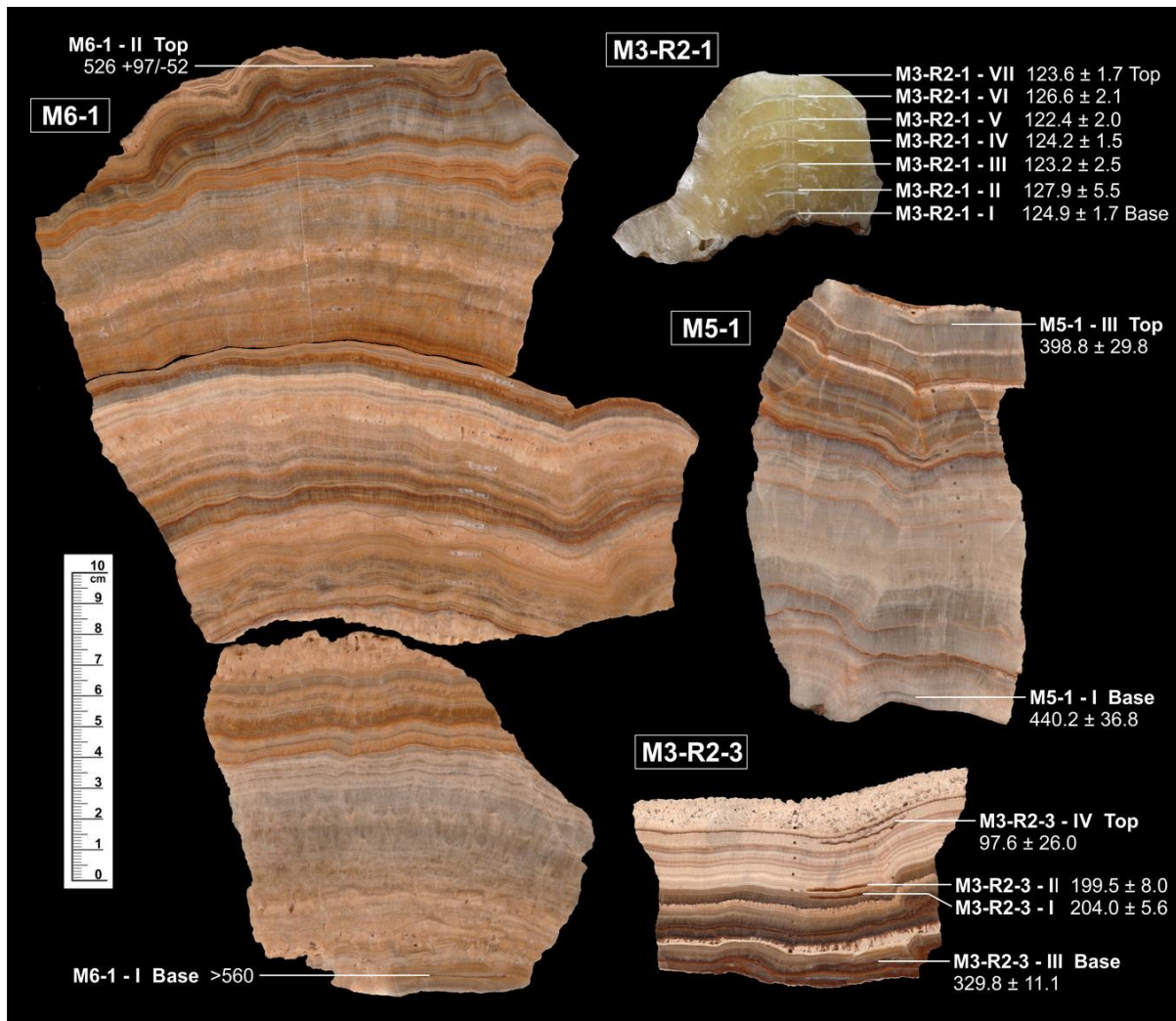
Figure 11. Sampling of speleothem calcite for U-Th dating and stable isotope analysis. Sample names are bolded, and the ages with corresponding uncertainties are given in ka. (2-column fitting image)

4.5. Stable isotope results

In stalagmite M3-R2-1, δ^{13}C values range between a minimum of -8.51‰ and a maximum of -6.05‰. In flowstone M3-R2-3 values range between -9.96‰ and -4.11‰, with an exceptional value of -2.70‰ measured within a moonmilk layer. Flowstone M5-1 has values between -9.30‰ and -4.49‰. The values of δ^{13}C in the host rock are positive, around 1‰: 1.15±0.04‰ in M5-3, 0.87±0.03‰ in M3-R2-1, and 1.49±0.07‰ in M3-R2-2.

31

4.6. Age and pollen content of D2 doline (M6 Cave) infill

The sedimentary infill of ridge-top doline D2 down to the depth of 2.10 m consists in three distinct layers (I-III) separated by brownish-black clayey horizons (Fig. 12). Three global samples analyzed for grain size, one from each layer (M6.a, M6.b, and M6.c), were plotted on pie charts. Grain size analysis shows a slight increase in clay content (11% to 15%) and decrease of sand (53% to 43%) downwards. The lower layer III (cm 210-110 on the profile) is a 1-m thick, fine-grained massive sediment with very loose rock fragments. The middle layer II (cm 110-75) contains denser and larger lithoclasts of 5-20 cm in size, and is overlain by a 5-cm thick black clayey layer. The upper layer I (cm 70-15) contains more sand compared to lower layers. The greenschist clasts are angular or subangular, whereas the marble clasts are either subangular or subrounded. A 15-cm regosol is developing atop of the sedimentary deposit.

Radiocarbon dating of the three samples returned ^{14}C age estimates that are in stratigraphic order: 2,589±28 years BP, 1,221±26 years BP, and 1,069±26 years BP. The calibrated ages, reported at 95.4% probability level, are as follows: between 2.77 and 2.55 ka for M6-19, between 1.26 and 1.07 ka for M6-10, and between 1.05 and 0.93 ka for M6-4.

In sample M6-14, a total of 250 pollen grains were counted and identified (excluding spores) along with 42 coniferous fragments *(Pinus/Picea)*. The pollen is dominated by alpine steppe taxa: *Asteraceae* (44%), *Poaceae* (20%), *Cyperaceae* (18%), and *Apiaceae* (4%). The arboreal taxa are represented by *Alnus* (14%), *Tilia* (2%), and the coniferous fragments. As well, the *Ericaceae* family taxa represent 4% of the total identified pollen grains.
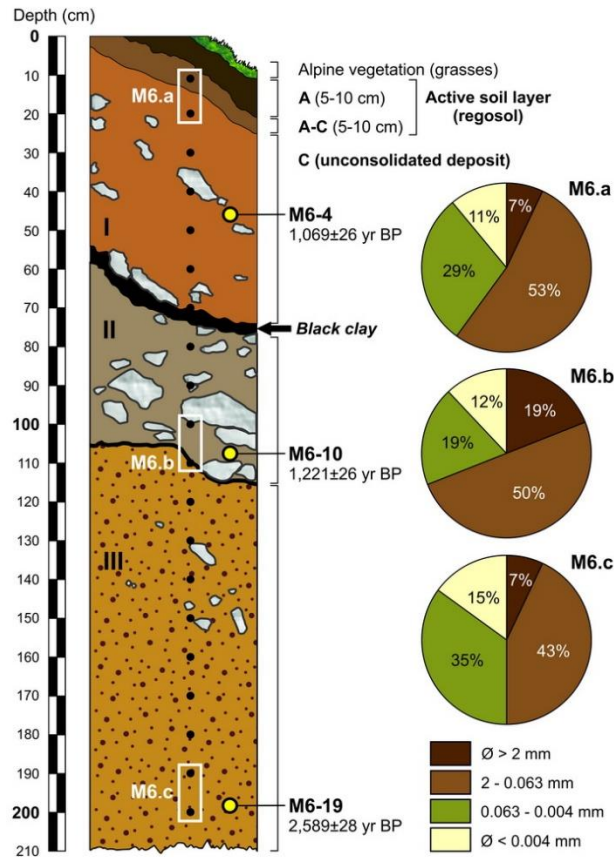
Figure 12. Sediment profile showing position of the analyzed samples and basic stratigraphy. The sediment is sloping from left to right, towards the flat bottom of the doline. Black dots represent the sub-samples collected for grain size analysis, and the white rectangles indicate the three most representative global samples with their grain size percentage plotted on the charts to the right.   (1-column fitting image)

5. DISCUSSION

5.1. Relations between karst, glacial and periglacial processes

The last glaciation left recognizable geomorphic evidence in the Făgăraş Mountains (Urdea et al., 2011; Kuhlemann et al., 2013; Mîndrescu, 2016). The crest, headwall and bottom of the

33

Mușeteica relict cirque, like elsewhere, are well-defined features which evolved little since the last deglaciation, affected only by erosion and local gravitational unloading.

The higher occurrence of dolines and ponors on the cirque bottom delineates an important area of dissolution and water infiltration in a concentrated flow, and the probable existence of an organized subterranean network. The glacial infill of covered paleodolines would have been subsequently affected by subsidence due to underground drainage, a process often seen in glaciokarst landscapes (Veress, 2016; Veress et al., 2019). During the last glacial period, the fossil ridge-top caves (M3-R2, M4, M5, and M6), located in the area above the trimline, were not directly influenced by glaciers, being subjected only to periglacial processes.

Such caves most probably formed during interglacials, when waters were more aggressive and able to enlarge cave passages (Häuselmann et al., 2007). Glaciers do not have a significant impact on dissolution speleogenesis (Audra, 2001; Häuselmann et al., 2002), due to the saturation in Ca^{2+} ions of the subglacial waters via incorporation of finely ground calcite eroded by the glacier (Bini et al., 1998), and due to a smaller CO_2 concentration that should have originated only from the atmosphere, in the absence of soil.

Under the influence of cold surface temperatures, ice could have formed in the frontal parts of the caves, contributing to passage enlargement during freeze-thaw cycles. This might explain for example the morphological differences between the front and the back of the M1 Cave.

5.2. Structural control

The cirque distribution in the Mușeteica-Buda area is highly controlled by geological structure. Nested cirques are aligned at 2000 and 2250 m a.s.l. on the northern slope, leaning against interlayered marbles and schists. Mușeteica cirque is subsequent in relation to marble

structure (NE-SW strike, Fig. 5), whereas Râiosu cirque is consequent, with direct implications on their comparably different shapes and sizes.

Arrangement and shape of dolines and roches moutonnées, the plan shape of the dry valley, and kluftkarren development on the lower cirque bottom corresponds to orientations of local faults and fractures (Fig. 5). Dry valleys developed subsequently on foliation at the contact between marbles and silicate rock bands. The stepped profile of the main dry valley is due to numerous swallow-holes formed on the foliation planes, favoring the access of stream water into the underground.

Some faults and fractures fitting the major NE-SW and NW-SE orientations, which define the structural framework of the Făgăraş Mountains, were crucial for underground karst development. The frontal part of M3-R2 Cave and the former ridge-top cave remnants (one of which is M6 Cave) are aligned on the NW-SE fault which crosses through the Muşeteica peak (2442 m). Further two NW-SE-oriented fractures which cross perpendicularly on the Muşeteica cirque are tension fractures formed due to postglacial rebound and gravitational spreading, as suggested by the presence of a discrete sackung-like feature and the position of these fractures within the glacial cirque (Gutiérrez-Santolalla et al., 2005). However, the unloading fractures inherited some older dextral transpression faults formed during the Late Miocene (Maţenco and Schmid, 1999). Subsidiary fracture sets (WNW-ESE and NNE-SSW) are less abundant, but perceptible at regional and local scales.

Still, not all fractures have a tectonic trigger at the origin. Locally, where slope disequilibrium was reached due to glacial lateral sapping, followed by glacier retreat, it prompted massive rockslides oriented conformably to marble foliation.

5.3. Speleogenetic stages

35

The observed speleogenesis in this area consists of three development stages: 1) texture- and fabric-controlled dissolution on foliation planes and tension fractures; 2) structurally-controlled breakdown; 3) cave unroofing and sediment infilling.

5.3.1. *Texture- and fabric-controlled dissolution (M1 Cave) and distension (ridge-top caves)*

The importance of contact planes between banded minerals with different physical and chemical properties in metamorphic rocks as speleoinception horizons plays a similar role with that of bedding planes in sedimentary rocks (Lowe and Gunn, 1997). Mineral segregation and recrystallization followed the direction imposed by the tectonic stress during metamorphism on the penetrative S_2 foliation.

The caves developed in schistose impure marbles containing thin silicate bands which have controlled the spatial development of fissure aquifers inside the bedrock. The banded fabric determined primary calcite dissolution preferentially along the silicate-carbonate contact planes, intersected by faults or pinnate fractures. The weakness of mineral cohesion resulted in the development of plane-parallel systematic joints (J3), related to the S_2 foliation. Exhumation of the metamorphic rocks, followed by erosion, gradually released the pressure from the overburden, and probably caused the formation of J3 plane-parallel distension joints. Thereafter, the central role on conduit development seems to have been played by the tension fractures that cross marbles perpendicularly on the S_2 foliation. These fractures correspond to the J1 joint family, which is the dominant joint system in the regional tectonic system (Fig. 9). Evidence of pressure flow can only be observed in the M1 Cave, but none in the ridge-top caves. These caves could have developed by diffuse water infiltration along the joint network, although organized water flow at low discharge could have played a role. Where fissure aquifers were intersected by faults or fractures, these evolved into karst conduits as pressure tubes (M1 Cave).

5.3.2. Structurally-controlled breakdown

In a later stage, enlargement of karst conduits caused breakdown due to decreasing stability of the ceiling, as described by White and White (2000). Breakdown, comparable to rock dissolution, occurred preferentially along the marble-schist contacts. Schist bands on the cave ceilings or ceiling edges were found in M3-R2 and M1 caves, which are larger and their morphology is better highlighted. The process is active and contributes to enlargement of chambers and passages and even to passage unroofing (surface breakdown).

Development of M1 Cave progressed along two main directions: NW-SE and NE-SW, intersecting in a 90º angle, conformably to local fractures geometry. The NW-SE passage depicts mostly a breakdown morphology, which is abruptly replaced by a pressure tube morphology in case of the NE-SW passage (Fig. 4A). This change in cave morphology could be attributed to tectonics: distension caused breakdown, whereas compression (or transpression) favored pressure tubes forming.

The breakdown-dissolution couple has gradually determined subsurface karst development along the marble foliation planes, whereas the surface components are mostly represented by dolines with ponors. M1 Cave is an exception, because it opens out on a roche moutonnée, partially collapsed due to subsurface breakdown.

5.3.3. Truncation, unroofing, and sediment infilling

The entrance of the M3-R2 Cave hangs above the Râiosu cirque on the eastern slope of Mușeteica Mt, indicating it was truncated by slope retreat, which generated the present-day shape of the Râiosu upper basin. As well, morphology of the D2 doline is evidence that former cave passages (M6 Cave) collapsed and were filled with sediment washed in from the surrounding slopes. The sediment infill has preserved the collapse morphology and *in situ* speleothems.

All the studied caves except M1 are arranged into a very small, 5,500-m^2 area on the mountain ridge top (Fig. 5). M4 and M5 caves, located very close to each other (~15 m), were undoubtedly truncated as inferred from the existence of *in situ* flowstones outside their entrance. Given their close position, we propose that these caves are remnant segments of a single network, whose interconnecting passages are probably obstructed by breakdown and sediment infill. Dissolution by percolating water was favored by the local tension fracture system and slowly modeled the cave walls under lithologic control, producing alternating sharp edges on the silicate sheets and corrosion grooves on the marble bands. No scallops were observed on the passage walls, indicating the lack of pressure flow. During cold periods (both periglacial and glacial conditions), cryoclastic phenomena would have played a role in developing the joint network. Some dissolution of weathering and breakdown material during warmer and wetter climate phases might have contributed to cave development, a process which can be observed today. On the contrary, there is no evidence for an old age or truncation of the M1 Cave.

5.4. Speleothem growth phases

Overall, the chronology of speleothem growth is generally well constrained given the limitations of the U-Th dating method. The largest age errors given by flowstones M6-1 and M5-1 are due on the one hand to the very low uranium content (between 14 and 51 ng/g), and on the other to the closeness of the U-Th dating limit, of ~500,000 years.

Speleothem formation seems to have occurred during at least five distinct phases (or episodes). The *first phase* was recorded by flowstone M6-1, which started growing before 560 ka, although this age estimate does not benefit from error assessment. The top of this flowstone has an age of 526 ka with an error defined as +97/-52 ka, which is not unusual for samples of similar age and with such low uranium content. A *second phase* is identified in

38

flowstone M5-1, which appears to have grown between 440 ±37 ka and 399 ±30 ka, roughly overlapping marine isotope stages 10 to 13 if uncertainties are considered in full. The *third phase* took place during MIS 9 and is identified at the base of sample M3-R2-3, at 330 ±11 ka. Also, in flowstone M3-R2-3, we can identify the *fourth phase* around 200 ka. Here, a change in petrography from dark brown to white, opaque calcite is defined by two age estimates of 204 ±6 ka and 200 ±8 ka, during MIS 7a-7c. Taking into account the error estimates, there could have been no hiatus at all between them, or a hiatus of at most 14 ka. One could speculate that it might have been caused by detrimental environmental conditions for speleothem formation during MIS 7b. A *fifth phase* is clearly defined by stalagmite M3-R2-1, which grew only during the warmest part of the last interglacial (MIS 5e), between 124.9 ±1.7 ka and 123.6±1.7 ka (Drăguşin, 2013). Moreover, the top of flowstone M3-R2-3 was dated at 97.6 ±26.0 ka, restricting its deposition to sometimes during MIS 5.

The U-Th ages fall mostly within interglacials (MIS 9, 7, and 5), except for M6-1 and possibly M5-1, where large age uncertainties hamper a good chronological control (Fig. 13). M3-R2-3 seems to even span several glacial cycles and we suspect that there should be hiatuses within the sample that cover the intervening glacial periods.

This might be due to the fact that mid-latitude speleothems form generally during interglacials, whereas formation ceases during glacials (Gordon et al. 1989; Baker et al. 1993; Lauritzen, 1995; Hercman, 2000; Spötl et al., 2007). Continuous deposition throughout glacial periods is characteristic only at circum–Mediterranean and sub–tropical sites (McDermott, 2004).

At sites similar to ours, for example at high elevation in the Alps, Spötl et al. (2002) and Holzkämper et al. (2005) showed that speleothems formed only during interglacials. Similarly, Norwegian speleothems were found to have formed during interglacials (Lauritzen et al., 1990; Lauritzen, 1995; Berstad et al., 2002; Lauritzen and Lundberg, 2004). In Søylegrotta (N Norway), the formation of stalagmite SG92-2 was restricted to MIS 15, 13,

11, and 9 (Berstad et al., 2002). Also in N Norway, flowstone LP6 from Laphullet Cave grew mostly during the MIS 11 interglacial (Lauritzen et al., 1990; Lauritzen and Lundberg, 2004). This speleothem is very similar with our sample M3-R2-3 with respect to its geomorphological and climatic setting. Laphullet Cave developed on a ridge-top in marble bedrock in an area with mean annual temperature of 2.8°C, near the Arctic Circle, and was repeatedly affected by glacier advance and retreat.
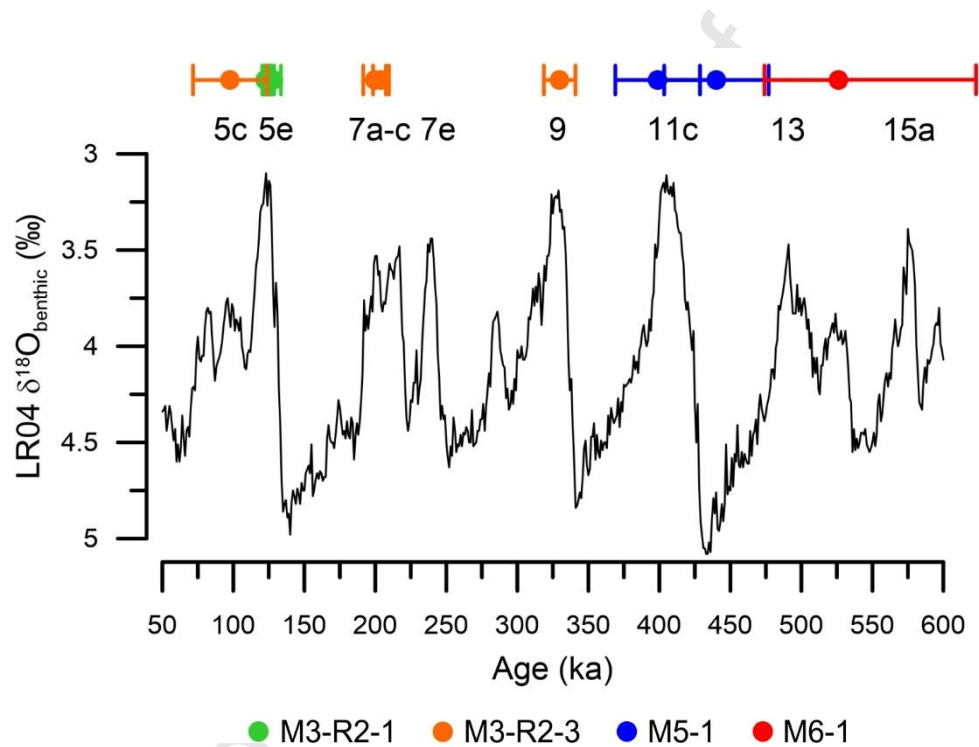

Figure 13. U-Th dates and their respective error bars from speleothems and the benthic $\delta^{18}O$ record of Lisiecki and Raymo (2005) in black. Marine isotope stages representing interglacials and their warming peaks are indicated by odd numbers and accompanying letters below the age plots. For the M6-1 flowstone, only the top age is shown, as the bottom age was out of U-Th dating range.   (1.5-column fitting image)

Stable carbon isotope values ($\delta^{13}C$) from these speleothems can help in discerning if calcite was deposited during warm periods, when soil plant and microbial activity were high, for example during interglacials. In our speleothems the lowest values are close to -10‰. They

can be the result of a mixing between organically derived CO_2 which usually has a $\delta^{13}C$ value of about -23‰ (in a C3 dominated plant association), and carbonate host rock (around 1‰ in our case), which usually gives a $\delta^{13}C$ speleothem value of around -11‰ (see for example the review work of McDermott, 2004). The highest values that we measured can be given by a wide range of processes intervening between host rock dissolution and speleothem deposition, but is not the aim of this work to discuss them. The most important information we want to convey is that values of -10‰ cannot be produced in the absence of plant and soil microbial activity specific to warm periods.

5.5. Significance of clastic sediment infill

The young age of the sediment infill, inferred both from the direct radiocarbon dating of bulk organic matter but also from the failure of obtaining OSL ages, implies that the collapse of the M6 Cave ceiling took place very recently, during the Holocene or, in any case not during the last glaciation. If the collapse doline generated by ceiling collapse would have been exposed to intense periglacial conditions during a glacial period, it would have been filled with cryoclasts and largely expanded outwards, whereas what we see at the moment are vertical walls, some of them even retaining flowstones. The angular to subangular shape of silicate rock clasts found in the sediment indicates little or no transport, and therefore an *in situ* gravitational infill following the cave ceiling collapse. Further excavation of the sediment in order to reach the bottom of the deposit will shed more light onto the collapse and sedimentation processes. At the moment we see no explanation for the infill provenance in such high quantities in such a short time interval.

Pollen preservation is rather poor given the presence of many degraded and unidentified degraded grains (15%), and a rather low number of taxa. Nevertheless, the sediment infill of the M6 Cave (doline D2) provides a good opportunity for future studies on vegetation

reconstructions considering the abundance of grains. The availability of large sample amounts that could be analyzed for a wide range of biogeochemical proxies offers an opportunity that is not available for the study of lake sediments, that relies on coring, and could be a welcomed addition to such type of Holocene archives from high elevation.

Further improvements in pollen and spore retrieval could be achieved by changes in the preparation protocol (e.g., removing the acetolysis step and reducing the HF treatment).

5.6. Regional landscape evolution and reconstruction of cave assemblage

The U-Th ages of our speleothems indicate that underground voids developed in the Mușeteica area before ~560 ka. As the sample yielding this age was retrieved from a wall, it also shows that this section of M6 Cave did not suffer from breakdown processes since its formation.

Evolution of the Mușeteica caves in a cold, glaciated environment was most likely dependent on surface erosion (via cirques development and increased lateral migration of the crests under the ice dynamics), coupled with water availability and soil development. The most important effect on surface topography was glacial and periglacial modelling, counterbalanced by mountain tectonic uplift, and to a lesser extent by fluvial erosion and marble dissolution.

5.6.1. Glacial erosion

The morphology of the Mușeteica glacial cirque itself is likely the result of several glacial phases during the Pleistocene. Studies have shown that the necessary time for cirques to form may be between 125 ka and beyond 400 ka (Barr and Spagnolo, 2015, and references therein). Therefore, it is likely that the glaciers have eroded the bedrock at least during the penultimate glaciation, MIS 6 (191-130 ka), and the Last Glacial Period, MIS 4-2 (70-12 ka).

The exact time of ice formation during the LGP is unknown. Based on the widely accepted fact that speleothems grow mostly during the interglacials/warm periods, and that our youngest speleothem age is 97.6±26.0 ka, we presume that local glaciation should have initiated sometimes between 115 and 70 ka. However, isotopic studies have shown that conditions for ice formation or advance were met mostly towards ~70 ka, given that the last warming peak of the MIS 5 interglacial (5a) was at 82 ka (Lisiecki and Raymo, 2005). The approximate age of deglaciation in the nearby cirques was around 12 ka (Kuhlemann et al., 2013). We can estimate that, over the cumulated intervals of the penultimate and last glaciations (~120 ka), glacial erosion could have removed a maximum of 72 m of bedrock, resulting in an average erosion rate of 0.6±0.02 mm yr^{-1}. If the Muşeteica glacier melted earlier than 12 ka, then we may allow for a slightly higher value of the glacial erosion rate, probably no more than 0.65 mm yr^{-1}. Temperate glaciers are able to erode the bedrock at rates between 0.1 and 10 mm yr^{-1} (Swift et al., 2015, and references therein). In the European Alps, Valla et al. (2011) have shown a minimum mean erosion rate of 1 mm yr^{-1}. Yet, the Alpine glaciers are better developed and more aggressive compared to former Carpathian glaciers, considering the cirque size of the latter (Mîndrescu and Evans, 2014).

5.6.2. Estimation of dissolution rates

During periods with no glacier presence, the dominant processes which might have lowered the topographic surface were karst dissolution and fluvial erosion. These processes must have contributed considerably less than the glaciers to surface erosion.

Regarding dissolution rates, Bögli (1971) reported values between 0.014 and 0.071 mm yr^{-1} for the bare karst in Muotatal (Switzerland), while Lauritzen (1990) found values between 0.013 and 0.023 mm yr^{-1} for Norway karst. For a moderate climate with effective precipitation of 1000 mm yr^{-1} and bare karst area, Gabrovšek (2007) has calculated a limestone dissolution rate of 0.04 mm yr^{-1}. At Innerbergli in the Swiss Alps, under climatic

43

and karst conditions similar to those in the Făgăraş Mountains, the average value is 0.014 ± 0.007 mm yr^{-1} (Häuselmann, 2008). According to these studies, marble dissolution rates do not exceed 0.1 mm yr^{-1} in such conditions, much lower than our calculated glacial erosion rate of ~0.6 mm yr^{-1}.

5.6.3. Mountain uplift estimates

Mountain uplift rates covering the Pleistocene epoch were not reported to date. Significant uplift events during the Upper Badenian, Upper Sarmatian, and uppermost Pannonian were recorded in the sediments of southern Transylvanian Basin, as shown by the sequence stratigraphy results (Maţenco et al., 2010), and show average uplift rates of 1, 0.8, and 1.88 mm yr-1, respectively. Modern geophysical measurements indicate higher uplift rates of 2-3 mm yr^{-1} (Zugrăvescu et al., 1998). Despite the apparent increase of the uplift rates since the Upper Miocene until present, such a large time gap confines the arguments on paleoaltimetry only to rough estimations, and therefore we excluded it from the proposed scenario below.

5.6.4. Sequence chronology of cave development and landscape evolution

The scenario proposed below is based on speleothem ages, and the assumption that the caves must be older than the deposits within. We describe six time periods in the evolution of this landscape during the past >560 ka, illustrated in Figure 14:

I) **Before ~560 ka.** The minimum estimated age of M6 Cave is provided by the U-Th dates of M6-1 sample, falling roughly within the MIS 15-13 interglacial. At this point, there is no evidence about the existence of any other cave nearby.

II) **At ~400 ka.** Most probably during the MIS 11 interglacial, M5 Cave was already formed and was probably longer, allowing for the deposition of flowstone M5-1. No datable cave deposit from the M4 Cave could provide insights into its age.

44

III) At ~330 ka. The first evidence for the existence of M3-R2 Cave during MIS 9 was the commencement of M3-R2-3 speleothem growth. Meanwhile, the intervening surface erosion, enhanced during the cold periods by glacial/periglacial conditions, should have thinned the overburden of M6 and M5 caves.

IV) At ~70 ka. Speleothems grew during the last interglacial perhaps only in the M3-R2 Cave. So far, we found no evidence of speleothem formation at this stage in the other ridge-top caves (M4, M5, or M6); therefore, we may assume that these caves had already been strongly truncated by erosion at that time, and speleothem growth was not possible anymore in the nearly exposed passages or chambers.

V) Last Glacial Period (~70 ka – 12 ka). The area above the trimline was subjected to periglacial processes, being close to erasing all the cave passages from the ridge. The Muşeteica glacier has removed a large amount of bedrock and dropped the altitude of land surface by a maximum of ~70 m. M1 Cave was probably invaded by ice in its frontal part, causing extensive breakdown, and received periodically a water influx from the glacier above, which subsequently modelled the tube in the back section.

VI) Late Holocene. Mountain uplift and erosion resulted in the present-day morphology and altitudes. The landscape should not have changed too much since the last deglaciation, except for gravitational spreading and partial modeling of karst landforms and glacial deposits. The ridge-top caves are subjected to slow dissolution, and passage enlargement by breakdown. M1 Cave is no longer enlarged by water flow under pressure, but shows multiple evidence of wall modelling by condensation corrosion in its frontal part. The roof of M6 Cave probably collapsed during the Holocene and was filled with clastic sediments washed from the nearby slopes, and is capped by active soil layers.
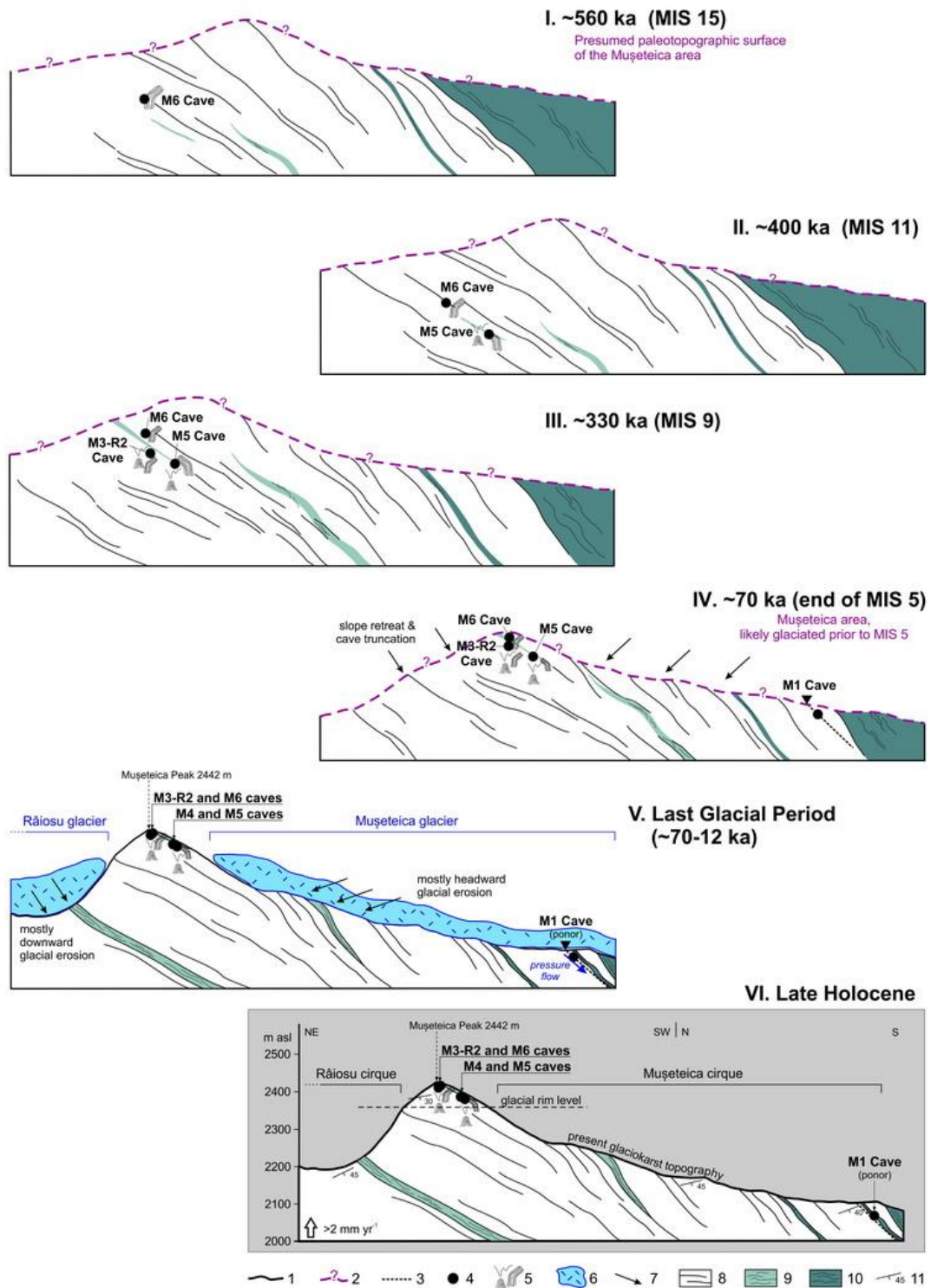
Figure 14. Evolution scenario of the Muşeteica glaciokarst: 1 – surface topography; 2 – hypothetical paleotopography; 3 – cave section; 4 – truncated cave; 5 – speleothem; 6 – mountain glacier; 7 – slope erosion; 8 – marble; 9 – greenschist; 10 – amphibolitic schist; 11 – strike and dip of rock foliation. (2-column fitting image)

46

The interpretation regarding the progress of glacial erosion illustrated in Figure 14 is based on a geomorphological foundation. Morphometry of the glacial cirques suggests that erosion progressed rather headward in the Muşeteica cirque, whereas in the smaller cirques around it (including the Râiosu cirque to the east) it acted mostly downward at least during the last glacial period. The hosted ice could not have removed enough material from the bedrock of these small cirques to force a significant headwall erosion compared to Muşeteica cirque. Here, the former glacier seems to have described a clockwise 70º–90º rotation from south towards the east, imposed by the geological structure of marbles.

6. CONCLUSIONS

This study provides new geomorphological and geochronological information on the evolution of the Făgăraş Mountains (Romania) marble karst and gives new insights into the relationship between karstification and Pleistocene environmental changes in the central South Carpathians. Our results show how the alpine karst and sedimentary archives such as speleothems and clastic infills have recorded these changes in an isolated high-altitude setting.

Geological structure seems to have controlled the spatial development of karst and glacial landforms, primarily through the layered structure of calcite marbles and the preferred orientation of faults and fractures. The primary tectonic directions are NE-SW and NW-SE, while WNW-ESE and NNE-SSW are secondary. Cave formation was related to four joint families measured on the marble bedrock, with the NW-SE-striking joint family being dominant in the entire area.

The Muşeteica glaciokarst contains two distinct zones: a) *the level above the trimline* comprises collapse dolines and cave remnants with speleothems; b) *the glacial cirque* hosts solution dolines, dry valleys, ponors, kluftkarren, a valley-bottom cave lacking speleothems

(M1 Cave), roches moutonnées, and plucked slope facets. Morphological evidence and lack of speleothems suggest that the M1 Cave is younger than the caves above the trimline and developed under the glacier during the last glaciation (MIS 4–2).

The ridge-top caves and former passages were truncated due to slope retreat under glacial and periglacial erosion, throughout the Middle and Late Pleistocene. We discovered a cave remnant (M6) by excavating the siliciclastic sediment infill of a ridge-top doline.

Three speleogenetic stages were outlined: 1) texture- and fabric-controlled dissolution and distension; 2) structurally-controlled breakdown; 3) cave truncation, unroofing, and sediment infilling.

We reported the first speleothem U–Th dates from the alpine karst in the Romanian Carpathians, that range between ~70 ka and more than 560 ka, spanning the Middle and Late Pleistocene. U-Th dating shows that speleothem deposition was limited mostly to interglacial periods. Stable carbon isotope values of these speleothems have a minimum around -10‰, indicating the presence of sustained activity from plant and soil microorganisms, consistent with environmental conditions of warm periods.

Based on speleothem ages and glaciokarst geomorphology, we proposed a landscape reconstruction scenario comprising six time slices, at >560 ka, 400 ka, 330 ka, 70 ka, 70 to 12 ka, and at present. Each chronological sequence illustrates changes that occurred in cave development, speleothem growth, and glacial/periglacial erosion.

The sediment accumulation we identified in the ridge-top dolines has a late Holocene age, preliminary radiocarbon dating showing it started depositing before ~3 ka. We showed that it preserved pollen from a mostly herbaceous plant association. Combined with other biogeochemical proxies and a possibility for large sample availability, these sedimentary archives can be a welcome complement to lake sediment cored from the region.

Acknowledgements

References

Ardelean, M., 2010. Piule-Iorgovanu Mountains: A geomorphology study. Ph.D. Thesis, Babes-Bolyai University, Cluj-Napoca, Romania (in Romanian).

Audra, P., 2001. French Alps Karst: study methods and recent advances. In: Häuselmann, P., Monbaron, M. (Eds.), Cave Genesis in the Alpine Belt. Proceedings of the 1st Workshop for Alpine Speleogenesis, Habkern (Switzerland), 10-13 September, 2000. Institute of Geography, University of Fribourg, pp. 7–28.

Baker, A., Smart, P.L., Ford, D.C., 1993. Northwest European palaeoclimate as indicated by growth frequency variations of secondary calcite deposits. Palaeogeogr. Palaeocl. 100 (3),

291–301. https://doi.org/10.1016/0031-0182(93)90059-R.

Balintoni, I., 1986. Considerations on a preliminary structural model of the South Carpathian crystalline east of the Olt river. D. S. Inst. Geol. Geofiz. 70–71 (5), 23–44.

Balintoni, I., Pană, D., 1993. Geology of the Făgăraş Mountains crest area between the Negoiu and Tătaru peaks. Rom. J. Tect. Reg. Geol. 75, 1–7 (in Romanian).

Balintoni, I., Balica, C., Ducea, M.N., Hann, H.-P., 2014. Peri-Gondwanan terranes in the Romanian Carpathians: A review of their spatial distribution, origin, provenance, and evolution. Geosci. Front. 5 (3), 395–411. http://dx.doi.org/10.1016/j.gsf.2013.09.002.

Ballesteros, D., Jiménez-Sánchez, M., Giralt, S., García-Sansegundo, J., Meléndez-Asensio, M., 2015. A multi-method approach for speleogenetic research on alpine karst caves. Torca La Texa shaft, Picos de Europa (Spain). Geomorphology 247, 35–54. http://dx.doi.org/10.1016/j.geomorph.2015.02.026.

Ballesteros, D., Giralt, S., García-Sansegundo, J., Jiménez-Sánchez, M., 2019. Quaternary regional evolution based on karst cave geomorphology in Picos de Europa (Atlantic Margin of the Iberian Peninsula). Geomorphology 336, 133–151. https://doi.org/10.1016/j.geomorph.2019.04.002.

Barr, I.D., Spagnolo, M., 2015. Glacial cirques as palaeoenvironmental indicators: their potential and limitations. Earth-Sci. Rev. 151, 48–78. https://doi.org/10.1016/j.earscirev.2015.10.004.

Berstad, I.M., Lundberg, J., Lauritzen, S.E., Linge, H.C., 2002. Comparison of the climate during marine isotope stage 9 and 11 inferred from a speleothem isotope record from northern Norway. Quaternary Res. 58 (3), 361–371. https://doi.org/10.1006/qres.2002.2387.

Beug, H.J., 2004. Leitfaden der Pollenbestimmung für Mitteleuropa und angrenzende Gebiete. Dr. Friedrich Pfeil Verlag, München, 542 p.

Bini, A., Tognini, P., Zuccoli, L., 1998. Rapport entre karst et glaciers durant les glaciations

dans les vallées préalpines du Sud des Alpes. Karstologia 32 (1), 7–26. http://dx.doi.org/10.3406/karst.1998.2422.

Bögli, A., 1971. Karstdenudation-das Ausmass des korrosiven Kalkabtrages. Regio Basiliensis 12 (2), 352–361.

Bronk Ramsey, C., 2009. Bayesian analysis of radiocarbon dates. Radiocarbon 51 (1), 337-360. https://doi.org/10.1017/S0033822200033865

Columbu, A., De Waele, J., Forti, P., Montagna, P., Picotti, V., Pons-Branchu, E., Hellstrom, J., Bajo, P., Drysdale, R., 2015. Gypsum caves as indicators of climate-driven river incision and aggradation in a rapidly uplifting region. Geology 43 (6), 539–542. https://doi.org/10.1130/G36595.1

Constantin, S., Robu, M., Munteanu, C.M., Petculescu, A., Vlaicu, M., Mirea, I., Kenesz, M., Drăguşin, V., Hoffman, D., Anechitei, V., Timar-Gabor, A., Roban, R., Panaiotu, C.G., 2014. Reconstructing the evolution of cave systems as a key to understanding the taphonomy of fossil accumulations: The case of Urşilor Cave (Western Carpathians, Romania). Quaternary International, 339-340, 25-40. http://dx.doi.org/10.1016/j.quaint.2013.10.012

Cooper, M.P., Mylroie, J.E., 2015. Glaciation and Speleogenesis: Interpretations from the Northeastern United States. Springer Int. Publishing, Cham, 142 p.

Dallmeyer, R.D., Neubauer, F., Fritz, H., Mocanu, V., 1998. Variscan vs. Alpine tectonothermal evolution of the Southern Carpathian orogen: constraints from $^{40}Ar/^{39}Ar$ ages. Tectonophysics 290, 111–135. https://doi.org/10.1016/S0040-1951(98)00006-7.

Dessila-Codarcea, M., Dimitrescu, R., Stancu, I., 1968. Geological map of Romania, scale 1:200,000. Sibiu sheet 27 (L-35-XIX). Geological Institute of Romania, Bucharest.

Dorale, J.A., Edwards, R.L., Alexander, E.C., Shen, C.-C., Richards, D.A., Cheng, H., 2004. Uranium-series dating of speleothems: Current techniques, limits, & applications. In: Sasowsky, I.D., Mylroie, J.E. (Eds.), Studies of cave sediments. Springer, Dordrecht, pp.

177–197.

Drăgușin, V., 2013. Late Pleistocene climate variability recorded in stalagmites from Romania. PhD Thesis. Babes-Bolyai University, Cluj-Napoca, 102 p.

Drăgușin, V., Mirea, I.C., Nae, A., Tîrlă, M.-L., 2019. Caves of the Făgăraș Mountains. In: Ponta, G.M.L., Onac, B.P. (Eds.), Cave and Karst Systems of Romania. Springer, Cham, pp. 79–82.

Federici, P.R., Spagnolo, M., 2004. Morphometric analysis on the size, shape and areal distribution of glacial cirques in the Maritime Alps (western French-Italian Alps). Geografiska Annaler Series A, Physical Geography 86 (3), 235–248. https://doi.org/10.1111/j.0435-3676.2004.00228.x.

Florea, M., 1998. Făgăraș Mountains: A geomorphological study. Foton Publ., Brașov, 114 p. (in Romanian).

Gabrovšek, F., 2007. On denudation rates in karst. Acta Carsologica 36 (1), 7-13.

Gee, G.W., Bauder, J.W., 1986. Particle-size analysis. In: Klute, A. (Ed), Methods of soil analysis: Part 1. Physical and Mineralogical Methods, 2nd Ed., Agronomy 9. Soil Science Society of America, Madison, USA, pp. 383–411.

Gheuca, I., 1988. Southern slope of the Făgăraș Mountains: lithostratigraphy and tectonics. D.S. Inst. Geol. Geofiz. 72–73 (5), 93–117 (in Romanian).

Giurgiu, I., 1990. The caves discovered at over 2000 m altitude, an essential addition to the image of the karst of Romania. Bul. CSER 13, 62–75 (in Romanian).

Giurgiu, I., 2006. The caves of Mușeteica. Invitație în Carpați 67, 28–57 (in Romanian).

Giușcă, D., Anastasiu, N., Popescu, G.C., Șeclăman, M., 1977. Remarks on the crystalline schists from the central Făgăraș Massif (Cumpăna − Cârțișoara Valley). An. Univ. Buc. (Geology) 26, 3–17 (in Romanian).

Gordon, D., Smart, P.L., Ford, D.C., Andrews, J.N., Atkinson, T.C., Rowe, P.J., Christopher, N.S.J., 1989. Dating of late Pleistocene interglacial and interstadial periods in the United

Kingdom from speleothem growth frequency. Quaternary Res. 31 (1), 14–26. https://doi.org/10.1016/0033-5894(89)90082-3.

Gutiérrez-Santolalla, F., Acosta, E., Ríos, S., Guerrero, J., Lucha, P., 2005. Geomorphology and geochronology of sackung features (uphill-facing scarps) in the Central Spanish Pyrenees. Geomorphology 69, 298–314. https://doi.org/10.1016/j.geomorph.2005.01.012.

Häuselmann, P., Jeannin, P.-Y., Monbaron, M., Lauritzen, S.-E., 2002. Reconstruction of Alpine Cenozoic paleorelief through the analysis of caves at Siebenhengste (BE, Switzerland). Geodin. Acta 15 (5–6), 261–276. https://doi.org/10.1080/09853111.2002.10510760.

Häuselmann, P., Granger, D.E., Jeannin, P.-Y., Lauritzen, S.-E., 2007. Abrupt glacial valley incision at 0.8 Ma dated from cave deposits in Switzerland. Geology 35 (2), 143–146. https://doi.org/10.1130/G23094A.

Häuselmann, P., 2007. How to date nothing with cosmogenic nuclides. Acta Carsologica 36 (1), 93–100. https://doi.org/10.3986/ac.v36i1.212.

Häuselmann, P., 2008. Surface corrosion of an Alpine karren field: recent measures at Innerbergli (Siebenhengste, Switzerland). Int. J. Speleol. 37 (2), 107–111. https://doi.org/10.5038/1827-806x.37.2.3.

Häuselmann, P., Mihevc, A., Pruner, P., Horáček, I., Čermák, S., Hercman, H., Sahy, D., Fiebig, M., Hajna, N.Z., Bosák, P., 2015. Snežna jama (Slovenia): Interdisciplinary dating of cave sediments and implication for landscape evolution. Geomorphology 247, 10–24. https://doi.org/10.1016/j.geomorph.2014.12.034.

Hellstrom, J., 2003. Rapid and accurate U/Th dating using parallel ion-counting multi-collector ICP-MS. J. Anal. Atom. Spectrom. 18, 1346–1351. https://doi.org/10.1039/B308781F.

Hercman, H., 2000. Reconstruction of paleoclimate changes in Central Europe between 10 and 200 thousand years BP, based on analysis of growth frequency of speleothems. Studia

Quaternaria 17, 35–70.

Hoffmann, D.L., Prytulak, J., Richards, D.A., Elliott, T., Coath, C.D., Smart, P.L., Scholz, D., 2007. Procedures for accurate U and Th isotope measurements by high precision MC-ICPMS. Int. J. Mass Spectrom. 264 (2-3), 97–109. https://doi.org/10.1016/j.ijms.2007.03.020.

Hoffmann, D.L., 2008. ^{230}Th isotope measurements of femtogram quantities for U-series dating using multi ion counting (MIC) MC-ICPMS. Int. J. Mass Spectrom. 275 (1-3), 75–79. https://doi.org/10.1016/j.ijms.2008.05.033.

Holzkämper, S., Spötl, C., Mangini, A., 2005. High-precision constraints on timing of Alpine warm periods during the middle to late Pleistocene using speleothem growth periods. Earth Planet. Sc. Lett. 236, 751–764. https://doi.org/10.1016/j.epsl.2005.06.002

Iancu, V., Berza, T., Seghedi, A., Gheuca, I., Hann, H.-P., 2005. Alpine polyphase tectono-metamorphic evolution of the South Carpathians: A new overview. Tectonophysics 410, 337–365. https://doi.org/10.1016/j.tecto.2004.12.038.

Klimchouk, A., Bayary, S., Nazik, L., Tork, K., 2006. Glacial destruction of cave systems in high mountains, with a special reference to the Aladaglar Massif, Central Taurus, Turkey. Acta Carsologica 35 (2), 111–121.

Kräutner, H.G., 1980. Lithostratigraphic correlation of Precambrian in the Romanian Carpathians. An. Com. Geol. Geofiz. LVII, 229–296.

Krijgsman, W., Piller, W.E., 2012. Regional stages in the Central and Eastern Paratethys. In: Gradstein, F.M., Ogg, J.G., Schmitz, M.D., Ogg, G.M. (Eds.), The Geologic Time Scale 2012, Vol. II. Elsevier, Amsterdam, pp. 935–937.

Kuhlemann, J., Dobre, F., Urdea, P., Krumrei, I., Gachev, E., Kubik, P., Rahr, M., 2013. Last Glacial Maximum glaciation of the Central South Carpathian range (Romania). Austrian J. Earth Sc. 106 (2), 50–62.

Lauritzen, S.- E., 1990. Autogenic and allogenic denudation in carbonate karst by the

multiple basin method: An example from Svartisen, North Norway. Earth Surf. Proc.
Land. 15 (2), 157–167. https://doi.org/10.1002/esp.3290150206.

Lauritzen, S.-E., Løvlie, R., Moe, D., Østbye, E., 1990. Paleoclimate deduced from a
multidisciplinary study of a half-million-year-old stalagmite from Rana, northern Norway.
Quaternary Res. 34 (3), 306–316. https://doi.org/10.1016/0033-5894(90)90043-K.

Lauritzen, S.-E., 1995. High-resolution paleotemperature proxy record for the last
interglaciation based on Norwegian speleothems. Quaternary Res. 43 (2), 133–146.
https://doi.org/10.1006/qres.1995.1015.

Lauritzen, S.-E., Lundberg, J., 2004. Isotope Stage 11, the "super-Interglacial", from a north
Norwegian speleothem. In: Sasowsky, I.D., Mylroie, J. (Eds.), Studies of Cave Sediments:
Physical and chemical records of paleoclimate. Springer, Dordrecht, pp. 257–272.
https://doi.org/10.1007/978-1-4419-9118-8_14.

Lauritzen, S.-E., 2001. Marble stripe karst of the Scandinavian Caledonides: An end-member
in the contact karst spectrum. Acta Carsologica 30/2 (3), 47–79.

Lisiecki, L.E., Raymo, M.E., 2005. A Pliocene-Pleistocene stack of 57 globally distributed
benthic $\delta^{18}O$ records. Paleoceanography and Paleoclimatology, 20, PA1003.
https://doi.org/10.1029/2004PA001071.

Lowe, D.J., Gunn, J., 1997. Carbonate speleogenesis: an inception horizon hypothesis. Acta
Carsologica 26 (2), 457–488.

Mais, K., 1999. Roofless caves, a polygenetic status of cave development with special
references to cave regions in the Eastern Calcareous Alps in Salzburg and Central Alps,
Austria. Acta Carsologica 28 (2), 145–158. https://doi.org/10.3986/ac.v28i2.489.

Maţenco, L., Bertotti, G., Dinu, C., Cloetingh, S., 1997. Tertiary tectonic evolution of the
external South Carpathians and the adjacent Moesian platform (Romania). Tectonics 16
(6), 896–911. https://doi.org/10.1029/97TC01238.

Maţenco, L., Schmid, S., 1999. Exhumation of the Danubian nappes system (South

Carpathians) during the Early Tertiary: inferences from kinematic and paleostress analysis at the Getic/Danubian nappes contact. Tectonophysics 314 (4), 401–422. https://doi.org/10.1016/S0040-1951(99)00221-8.

Maţenco, L., Krézsek, C., Merten, S., Schmid, S., Cloetingh, S., Andriessen, P., 2010. Characteristics of collisional orogens with low topographic build-up: an example from the Carpathians. Terra Nova 22, 155–165. https://doi.org/10.1111/j.1365-3121.2010.00931.x.

McDermott, F., 2004. Palaeo-climate reconstruction from stable isotope variations in speleothems: a review. Quaternary Science Reviews, 23 (7–8), 901-918, https://doi.org/10.1016/j.quascirev.2003.06.021.

Merten, S., 2011. Thermo-tectonic evolution of a convergent orogen with low topographic build-up: Exhumation and kinematic patterns in the Romanian Carpathians derived from thermochronology. Ph.D. Thesis, Vrije Universiteit, Amsterdam.

Meyer, M.C., Cliff, R.A., Spötl, C., 2011. Speleothems and mountain uplift. Geology 39 (5), 447–450. https://doi.org/10.1130/G31881.1.

Micalevich, V., 1959. Quelques éléments nouvels concernant l'établissement des phases glaciares du massif Bucegi. Probleme de Geografie VI, 219–226 (in Romanian, with French abstract).

Mihai, S., Moldoveanu, C., 2006. Muşeteica – Geomorphology. Invitaţie în Carpaţi 67, 58–63 (in Romanian).

Mîndrescu, M., 2016. Geomorphometry of glacial cirques in the Romanian Carpathians."Ştefan cel Mare" University Press, Suceava, 173 p. (in Romanian).

Mîndrescu, M., Evans, I.S., 2014. Cirque form and development in Romania: Allometry and the buzzsaw hypothesis. Geomorphology 208, 117–136. https://doi.org/10.1016/j.geomorph.2013.11.019.

Moore, P., Webb, J.A., Collinson, M.E., 1991. Pollen analysis, 2nd Ed. Blackwell Scientific Publications, Oxford, 216 p.

National Meteorological Administration, 2017. Mean monthly temperature and precipitation at Bâlea Lac weather station (1986-2016). Dataset. Bucharest, Romania.

Nedelea, A., 2006. Argeş Valley in the mountain sector: Geomorphology study. Bucharest University Press, Bucharest, 229 p. (in Romanian).

Niculescu, G., 1965. Godeanu Mountains: A geomorphological study. Academy Press, Bucharest, 339 p. (in Romanian).

Pană, D., 1990. Central and northern Făgăraş – Lithological sequences and structure. D. S. Inst. Geol. Geofiz. 74 (5), 81–99.

Passchier, C.W., Trouw, R.A.J., 2005. Microtectonics. Springer-Verlag, Berlin, 366 p. https://doi.org/10.1007/3-540-29359-0.

Piccini, L., 2011. Recent developments on morphometric analysis of karst caves. Acta Carsologica 40 (1), 43–52. https://doi.org/10.3986/ac.v40i1.27.

Polyak, V.J., McIntosh, W.C., Guven, N., Provencio, P., 1998. Age and origin of Carlsbad Cavern and related caves from ^{40}Ar/^{39}Ar of alunite. Science 279 (5358), 1919–1922. https://doi.org/10.1126/science.279.5358.1919.

Popescu, R., Urdea, P., Vespremeanu-Stroe, A., 2017. Deglaciation history of high massifs from the Romanian Carpathians: Towards an integrated view. In: Rădoane, M., Vespremeanu-Stroe, A. (Eds.), Landform Dynamics and Evolution in Romania. Springer, Cham, pp. 87–116. https://doi.org/10.1007/978-3-319-32589-7_5.

Răbăgia, T., Maţenco, L., 1999. Tertiary tectonic and sedimentological evolution of the South Carpathians foredeep: tectonic vs eustatic control. Mar. Petrol. Geol. 16 (7), 719–740. https://doi.org/10.1016/S0264-8172(99)00045-8.

Reimer, P.J., Bard, E., Bayliss, A., Beck, J.W., Blackwell, P.G., Bronk Ramsey, C., Grootes, P.M., Guilderson, T.P., Haflidason, H., Hajdas, I., Hatté, C., Heaton, T.J., Hoffmann, D.L., Hogg, A.G., Hughen, K.A., Kaiser, K.F., Kromer, B., Manning, S.W., Niu, M., Reimer, R. W., Richards, D.A., Scott, E.M., Southon, J.R., Staff, R.A., Turney, C.S.M.,

van der Plicht, J., 2013. IntCal13 and Marine13 radiocarbon age calibration curves 0-50,000 years cal BP. Radiocarbon, 55 (4), 1869–1887. https://doi.org/10.2458/azu_js_rc.55.16947.

Reuther, A., Urdea, P., Geiger, C., Ivy-Ochs, S., Niller, H.P., Kubik, P.W., Heine, K., 2007. Late Pleistocene glacial chronology of the Pietrele Valley, Retezat Mountains, Southern Carpathians, constrained by [10]Be exposure ages and pedological investigations. Quatern. Int. 164–165, 151–169. https://doi.org/10.1016/j.quaint.2006.10.011.

Richards, D.A., Dorale, J.A., 2003. Uranium-series chronology and environmental applications of speleothems. Rev. Mineral. Geochem. 52 (1), 407–460. https://doi.org/10.2113/0520407.

Ruszkiczay-Rüdiger, Z., Kern, Z., Urdea, P., Braucher, R., Madarász, B., Schimmelpfennig, I., 2016. Revised deglaciation history of the Pietrele–Stânişoara glacial complex, Retezat Mts, Southern Carpathians, Romania. Quatern. Int. 415, 216–229. https://doi.org/10.1016/j.quaint.2015.10.085.

Sasowsky, I.D., 1998. Determining the age of what is not there. Science 279 (5358), 1874–1874. https://doi.org/10.1126/science.279.5358.1874.

Sava, T., Simion, C., Gâza, O., Stanciu, I., Păceşilă, D., Sava, G., Wacker, L., Ştefan, B., Moşu, V., Ghiţă, D., Vasiliu, A., 2019. Status report on the Sample Preparation Laboratory for Radiocarbon Dating at the New Bucharest RoAMS Center. Radiocarbon 61 (2), 649–658. https://doi.org/10.1017/RDC.2018.123.

Schmid, S., Berza, T., Diaconescu, V., Froitzheim, N., Fügenschuh, B., 1998. Orogen-parallel extension in the Southern Carpathians. Tectonophysics 297 (1), 209–228. https://doi.org/10.1016/S0040-1951(98)00169-3.

Scholz, D., Hoffmann, D.L., 2008. [230]Th/U-dating of fossil corals and speleothems. E&G Quatern. Sci. J. 57, 52–76. https://doi.org/10.3285/EG.57.1-2.3.

Schuster, A.C., 1977. Geological map of Romania, scale 1:50,000. Negoiu sheet 109a (L-35-

86-A). Geological Institute of Romania, Bucharest.

Silvăşanu, G., 1982. A speleological trail in the Făgăraş Mountains. Buletin Speol. Inf. 6, 127–131 (in Romanian).

Smart, C., 2004. Glacierized and glaciated karst. In: Gunn, J. (Ed.), Encyclopedia of caves and karst science. Fitzroy Dearborn, New York, pp. 804–809.

Spötl, C, Mangini, A., Frank, N., Eichstädter, R., Burns, S.J., 2002. Start of the last interglacial period at 135 ka: Evidence from a high Alpine speleothem. Geology 30 (9), 815–818. https://doi.org/10.1130/0091-7613(2002)030<0815:SOTLIP>2.0.CO;2.

Spötl, C., Holzkämper, S., Mangini, A., 2007. The last and the penultimate interglacial as recorded by speleothems from a climatically sensitive high-elevation cave site in the Alps. In: Sirocko, F., Claussen, M., Sanchez-Goñi, M.F., Litt, T. (Eds.), The Climate of Past Interglacials. Elsevier, Amsterdam, pp. 471–491. https://doi.org/10.1016/S1571-0866(07)80056-X.

Stelea, I., 1992. Considerations upon the lithostratigraphy and metamorphism of the Făgăraş series. Rom. J. Petrol. 75, 183–188.

Stock, G.M., Riihimaki, C.A., Anderson, R.S., 2006. Age constraints on cave development and landscape evolution in the Bighorn Basin of Wyoming, USA. J. Cave Karst Stud. 68 (2), 76–84.

Swift, D.A., Cook, S., Heckmann, T., Moore, J., Gärtner-Roer, I., Korup, O., 2015. Ice and snow as land-forming agents. In: Shroder, J.F., Haeberli, W., Whiteman, C. (Eds.), Snow and Ice-Related Hazards, Risks, and Disasters. Elsevier, Amsterdam, pp. 167–199. https://doi.org/10.1016/B978-0-12-394849-6.00006-8.

Telbisz, T., Tóth, G., Ruban, D.A., Gutak, J.M., 2019. Notable glaciokarsts of the world. In: Veress, M., Telbisz, T., Tóth, G., Lóczy, D., Ruban, D.A., Gutak, J.M. (Eds.), Glaciokarsts. Springer, Cham, pp. 373–499.

Teodorescu, M.-A., Mitrofan, H., 1999. An alpine karst occurrence: Găuri Cirque (Parâng

Mountains, Romania). Theor. Appl. Karst. 11–12, pp. 169–176.

Tîrlă, L., Drăguşin, V., Mirea, I.C., Cojocaru, T., 2016. Speleomorphology of M3-R2 – The highest cave in the SE Carpathians. Revista de Geomorfologie, 18, 54–62.

Urdea, P., 2004. The Pleistocene glaciation of the Romanian Carpathians. In: Ehlers, J., Gibbard, P.L. (Eds.), Quaternary Glaciations – Extent and Chronology, Part 1: Europe. Elsevier, Amsterdam, pp. 301–308.

Urdea, P., Onaca, A., Ardelean, F., Ardelean, M., 2011. New Evidence on the Quaternary Glaciation in the Romanian Carpathians. In: Ehlers, J., Gibbard, P.L., Hughes, P.D. (Eds.), Quaternary Glaciations – Extent and Chronology: A Closer Look. Elsevier, Amsterdam, pp. 305–322.

Valla, P.G., Shuster, D.L., Van Der Beek, P.A., 2011. Significant increase in relief of the European Alps during mid-Pleistocene glaciations. Nat. Geosci. 4 (10), 688–692. https://doi.org/10.1038/ngeo1242.

Veress, M., 2016. Covered Karsts. Springer, Dordrecht, 536 p.

Veress, M., Telbisz, T., Tóth, G., Lóczy, D., Ruban, D.A., Gutak, J.M., 2019. Glaciokarsts. Springer, Cham, 516 p.

Wentworth, C.K., 1922. A scale of grade and class terms for clastic sediments. J. Geol. 30, 377–392.

White, E.L., White, W.B., 2000. Breakdown morphology. In: Klimchouk, A., Ford, D.C., Palmer, A.N., Dreybrodt, W. (Eds.), Speleogenesis: Evolution of Karst Aquifers. National Speleological Society, Huntsville, Alabama, pp. 427–429.

White, W.B., 2007. Cave sediments and paleoclimate. J. Cave Karst Stud. 69 (1), 76–93.

Žebre, M., Stepišnik, U., 2015. Glaciokarst landforms and processes of the southern Dinaric Alps. Earth Surf. Proc. Land. 40 (11), 1493–1505. https://doi.org/10.1002/esp.3731.

Zugrăvescu, D., Polonic, G., Horomnea, M., Dragomir, V., 1998. Recent vertical crustal movements on the Romanian territory, major tectonic compartments and their relative

dynamics. Rev. Roum. Géophys. 42, 3–14.

Abstract

The Carpathian island-type glaciokarst has a great potential of preserving signals of past environments, archived in cave deposits like speleothems and clastic infills. We present here the geomorphology and structural control of several relict alpine caves and the surrounding glaciated marble karst in the Făgăraș Mountains. Four truncated and partially unroofed caves remained on the ridge-top of Mușeteica Mountain, above the glacial cirque, while a ponor cave that developed on the cirque bottom could be related to the Last Glacial Period. Structural measurements and cave morphology showed that the conduits formed at the intersection of foliation planes and tectonic fractures on the NE-SW and NW-SE directions. Cave development reflects three speleogenetic stages: 1) texture- and fabric-controlled dissolution and distension; 2) structurally-controlled breakdown; and 3) truncation, unroofing, and cave infilling with sediments. Slow diffuse dissolution was typical for the ridge-top caves, whereas M1 Cave developed by pressure flow.

Further, we report the first U-Th speleothem ages, related to the evolution of alpine caves and island glaciokarst in the South Carpathians during the Middle and Late Pleistocene. Dating results show a minimum estimated age of ~560 ka for the ridge-top caves, and that speleothem deposition met optimal conditions only during warmer periods, largely corresponding to interglacials. Stable carbon isotope values in speleothems range between -9.96‰ and -4.11‰, indicating the presence of plant and soil organic activity at the time of deposition. In total, five speleothem growth phases were distinguished during the last ~560 ka.

We excavated the sediment infill of a ridge-top doline down to a 2-m depth. Radiocarbon dating revealed that it was deposited during the Late Holocene, and preliminary pollen analysis identified a plant assemblage dominated by grasses.

Using the relationships between karst development, glaciation, and cave sedimentary archives, we present a time slice chronology of alpine landscape evolution at >560 ka, ~400 ka, ~330 ka, the Last Glacial Period (70-12 ka), and the Late Holocene. Our geomorphological, isotopic, and geochronological results also support the existing hypothesis that the South Carpathians may have experienced at least two glacial phases during the Pleistocene. Glacial erosion rate during the Last Glacial Period, and most likely during the penultimate glaciation, averages around 0.6 mm yr^{-1}.

Keywords:

Carpathians; Speleothem; Glaciated karst; High-altitude cave.

Declaration of interests

☒ The authors declare that they have no known competing financial interests or personal relationships that could have appeared to influence the work reported in this paper.

☐The authors declare the following financial interests/personal relationships which may be considered as potential competing interests:
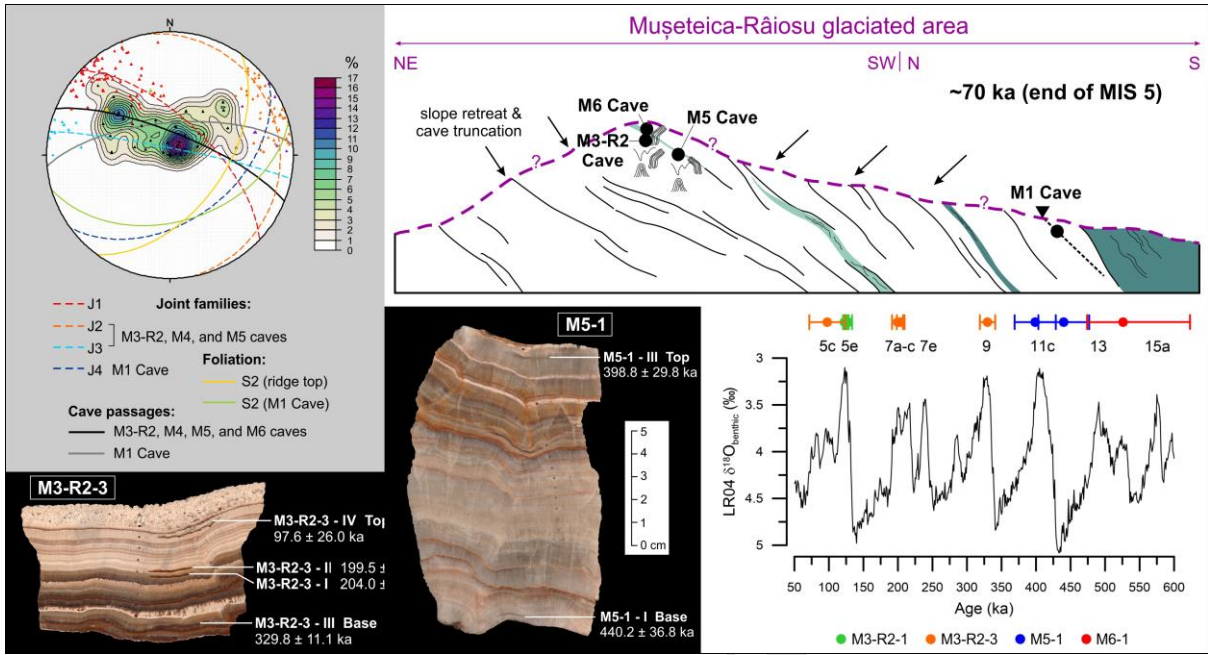
Graphical abstract

Highlights

- We investigated glaciokarst morphology in the Făgăraș Mountains, Romania

- We provide the first speleothem ages of alpine caves in the South Carpathians

- The minimum estimated age of ridge-top caves is ~560 ka

- Speleothem growth was limited only to warm periods

- Sedimentary infill of dolines unravels Late Holocene environmental conditions